DEVELOPMENT AND CHARACTERIZATION OF AN INTRACORTICAL CLOSED-LOOP BRAIN-COMPUTER INTERFACE

by

Jeffrey M. Weiss

B.S. in Bioengineering, University of Pittsburgh, 2013

Submitted to the Graduate Faculty of

the Swanson School of Engineering in partial fulfillment

of the requirements for the degree of

Master of Science

University of Pittsburgh

2018

UNIVERSITY OF PITTSBURGH

SWANSON SCHOOL OF ENGINEERING

This thesis was presented

by

Jeffrey M. Weiss

It was defended on

March 19, 2018

and approved by

Jennifer Collinger PhD, Assistant Professor, Department of Physical Medicine and Rehabilitation, University of Pittsburgh

Robert Gaunt PhD, Assistant Professor, Department of Physical Medicine and Rehabilitation, University of Pittsburgh

Patrick Loughlin PhD, Associate Professor, Department of Bioengineering, University of Pittsburgh

Thesis Advisor: Jennifer Collinger PhD, Assistant Professor, Department of Physical Medicine and Rehabilitation, University of Pittsburgh

DEVELOPMENT AND CHARACTERIZATION OF AN INTRACORTICAL CLOSED-LOOP BRAIN-COMPUTER INTERFACE

Jeffrey M. Weiss, M.S.

University of Pittsburgh, 2018

Intracortical brain-computer interfaces (BCI) have the potential to restore motor function to people with paralysis by extracting movement intent signals directly from motor cortex. While current technology has allowed individuals to perform simple object interactions with robotic arms, such demonstrations have depended exclusively on visual feedback. Additional forms of sensory feedback may lessen the dependence on vision and allow for more dexterous control. Intracortical microstimulation (ICMS) has been proposed as a method of adding somatosensory feedback to BCI by directly stimulating somatosensory cortex to evoke tactile sensations referred to the hand. Our lab recently demonstrated that ICMS can elicit graded and focal tactile sensations in an individual with spinal cord injury (SCI). However, several challenges must be resolved to demonstrate the viability of ICMS as a technique for incorporating sensory feedback in a closed-loop BCI.

First, microstimulation generates large voltage transients that appear as artifacts in the neural recordings used for BCI control. These artifacts can corrupt the recorded signal throughout the entire stimulus train, and must be eliminated to allow for continuous BCI decoding. Second, it is unknown whether the sensations elicited by ICMS can be perceived quickly enough for use as a feedback signal.

Here, I present several aspects of the development of a closed-loop BCI system, including a method for artifact rejection and the characterization of simple reaction times to ICMS of human somatosensory cortex. A human participant with tetraplegia due to SCI was implanted with four microelectrode arrays in primary motor and somatosensory cortices.

I implemented a robust method of artifact rejection that preserves neural data as soon as 750 microseconds after each stimulus pulse by applying signal blanking and an appropriate digital filter. I validated this method by comparing BCI performance with and without ICMS and found that performance was maintained with ICMS and artifact rejection. Next, I characterized simple reaction times to single-channel ICMS, and found that responses to ICMS were comparable, and often faster, than responses to electrical stimulation on the hand. These findings suggest that ICMS is a viable method to provide feedback in a closed-loop BCI.

TABLE OF CONTENTS

LIST OF TABLES

LIST OF FIGURES

PREFACE

I first discovered the field of neural engineering when a video from Dr. Andrew Schwartz's lab was shown to my undergraduate Bioengineering seminar. The video depicted a monkey using a brain-computer interface (BCI) to control a robotic arm and feed himself marshmallows. At this point in my education, I was unsure if I had even made the right choice in being a Bioengineering major, but after discovering the field of BCI, I knew that I had to begin research in neural engineering. Throughout the remainder of my undergraduate career, my interest in neural engineering was fostered by the support of Dr. Doug Weber and Dr. Aaron Batista, as well as Dr. Jim Hokanson who dedicated far too many hours mentoring me while working on his PhD. Doug also recommended me for a staff engineering position at the Rehab Neural Engineering Lab (RNEL) after undergrad, which is where I got my start with intracortical BCI research. I have much gratitude for these three people for giving me a start in neural engineering.

I of course cannot thank my committee members enough for all the advice, wisdom and support they have provided over the years. My relationship with Dr. Patrick Loughlin began in undergrad, when he was my academic advisor. At the time I ignored him anytime he asked if I wanted to go to grad school, but after two years of working at the RNEL, Pat remained persistent in pushing me to apply. Before I knew it, I was a TA for Pat's Signals and Systems class.

I have worked as an engineer for Dr. Jennifer Collinger and Dr. Robert Gaunt for five years. Thanks to their encouragement, I have also been a part-time student for nearly three of those years. Sometimes the lines dividing my role as an engineer and student can be blurry, but at times my dual roles have been very difficult to manage. Thus, I must thank Jen and Rob for incredible patience as I have finished experiments, analyses, and papers later

than planned, or fixed bugs at a snail's pace. I must also extend this thanks to all RNEL members, including former PhD students Dr. John Downey and Dr. Sharlene Flesher, who helped with my transition to the lab and provided an abundance of support.

I would also like to thank my family for their support and motivation throughout my whole life (even though it proved harder to get a plug on my sister's late night show than from President Obama), and Alaina for encouragement and coffee while working through many nights and weekends.

And finally, I owe so much gratitude to Jan and Nathan, the two participants I have had the pleasure of working with in the BCI study. They have both showed incredible dedication to the progress of this field, so much that they have traveled three times a week, every week, for years to participate in experiments that aren't always as glamorous as the time Jan controlled two robot arms to play a Rock Band drumset (with no prior percussion experience), or the time Nathan made an actual painting (with no prior art experience). Thank you both for the fun, the laughs, and the motivation to continue making progress towards a take-home BCI device.

1.0 INTRODUCTION

Individuals with tetraplegia due to conditions such as spinal cord injury, strokes, or neurodegenerative diseases such as amyotrophic lateral sclerosis (ALS) are unable to use their hands or legs, and in many cases are paralyzed from the neck down. While assistive devices exist to help individuals with tetraplegia operate wheelchairs and computers, such individuals often require assistance for activities of daily living and struggle to be independent. Just as cochlear implants have restored hearing to individuals with deafness [Eshraghi et al., 2012], a neural prosthesis may be capable of restoring motor function and independence to individuals with paralysis.

In recent years, a number of advances in the field of brain-computer interfaces (BCI) have allowed people with paralysis to control robotic limbs using intent signals recorded from the motor cortex [Collinger et al., 2013, Downey et al., 2016, Wodlinger et al., 2014]. However, future progress may plateau without incorporating sensory feedback to reduce the reliance on visual feedback and allow for more dexterous object interactions. Intracortical microstimulation (ICMS) has been proposed as a method of introducing such feedback, but a number of challenges remain to be solved before the viability of this technique can be demonstrated. The efficacy of ICMS must be proven in the sense that the sensations produced by ICMS can be interpreted in a meaningful and timely manner as feedback to improve motor control. Furthermore, the addition of ICMS must not disrupt the existing components of a BCI system. In particular, care must be taken to ensure that the recording quality and motor control does not degrade with the addition of microstimulation.

In this chapter, I will provide background on BCI research, the somatosensory system and the need for somatosensory feedback in prosthetic devices, and ICMS, including the history, mechanism, effects, and safety of using microstimulation in the brain. I will also discuss

problems and unknowns with using ICMS in a BCI system, including stimulus artifacts and the response latency of ICMS, to motivate the novel work presented in this thesis. In Chapter 2, I will describe a method of removing stimulus artifacts and validate the method in a closed-loop BCI system. In Chapter 3, I will characterize the reaction times to ICMS, a first step in determining whether or not ICMS can transmit information quickly enough for use as feedback. Finally, I will summarize my findings and discuss alternative solutions and future work in Chapter 4.

1.1 BRAIN-COMPUTER INTERFACE

A brain-computer interface (BCI) is a device that extracts signals from a user's brain to control external devices. The concept was first proposed in 1973 by Jacques Vidal as a potential method of "controlling such external apparatus as prosthetic devices or spaceships" [Vidal, 1973]. While BCI spaceships are still relegated to science fiction,[1] research into brain-controlled prosthetics has made significant progress in recent years. Several methods exist for extracting brain signals for BCI, including the non-invasive electroencephalogram (EEG) (e.g. [Wolpaw et al., 1991]), and more invasive electrocorticography (ECoG) (e.g. [Leuthardt et al., 2004, Wang et al., 2013]) or intracortical microelectrode arrays (e.g. [Collinger et al., 2013, Hochberg et al., 2006]), both of which require implanted electrodes. While each of these technologies has unique benefits and limitations, this thesis will focus on intracortical BCIs that make use of implanted microelectrodes to record from single neurons.

In 1969, Eberhard Fetz performed an operant conditioning experiment that trained monkeys to modulate the firing rate of single units in motor cortex in order to receive a food reward [Fetz, 1969]. The monkeys received auditory or visual feedback corresponding to the firing rate of the recorded unit. This experiment demonstrated for the first time that it is possible to volitionally control the firing rates of individual neurons. A decade later, Edward Schmidt performed a similar experiment with the goal of controlling external devices by

[1] Elon Musk, the billionaire entrepreneur and founder of the commercial aerospace company SpaceX, co-founded Neuralink in 2016, which is reportedly working on invasive brain-computer interfaces [Urban, 2017]. One can only speculate about Musk's true intentions.

direct cortical control [Schmidt, 1980]. Schmidt trained monkeys to modulate firing rates of single units to eight discrete firing rate targets, indicated by a row of lightbulbs, and discussed the possibility of extracting signals from cortex to control external devices such as neuromuscular stimulators for people with quadriplegia.

A major breakthrough was made when Apostolos Georgopoulos discovered a method to decode movement direction from populations of neurons in motor cortex [Georgopoulos et al., 1982]. Georgopoulos recorded from single neurons while monkeys performed an eight-target center-out reaching task, and discovered that many neurons exhibited a "preferred direction" in which they fired maximally, and attenuated their firing rates during reaches in the opposite direction. A cosine tuning curve could be fit to relate the firing rate of each cell to movement direction. Georgopolous then repeated this experiment with three-dimensional reaches and developed the population vector algorithm, in which each cell was treated as a vector along the axis of its preferred direction. The firing rate of each cell was then used to determine a weighted contribution to a resultant population vector predicting the direction of the monkey's reach [Georgopoulos et al., 1986]. This algorithm eventually led to the development of BCI decoders [Schwartz et al., 2001], which translate neural firing rates into control signals for external devices.

By the early 2000s, microelectrode arrays had been developed that allowed many neurons to be recorded simultaneously. Several groups trained monkeys to control cursors [Serruya et al., 2002, Taylor et al., 2002] or robotic arms[2] [Carmena et al., 2003] by decoding velocity from populations of neurons in motor cortex. A few years later, Andrew Schwartz's group trained monkeys to control a robotic arm and hand with four degrees-of-freedom (endpoint position and grasp) in a self-feeding task [Velliste et al., 2008].

During this time, intracortical BCI began translating to clinical human work. The "BrainGate" clinical trial demonstrated that humans with tetraplegia could use a BCI to control a cursor and interact with a computer [Hochberg et al., 2006], and that the system could function for at least 1000 days [Simeral et al., 2011]. This clinical trial involved implanting a Utah electrode array (as seen in Figure 1.1), a 4x4 mm array of 100 microelectrodes which

[2]In the cited study, monkeys learned to control a cursor with a BCI. The BCI was then used to control a robot, but the monkeys were only presented with a cursor for visual feedback.

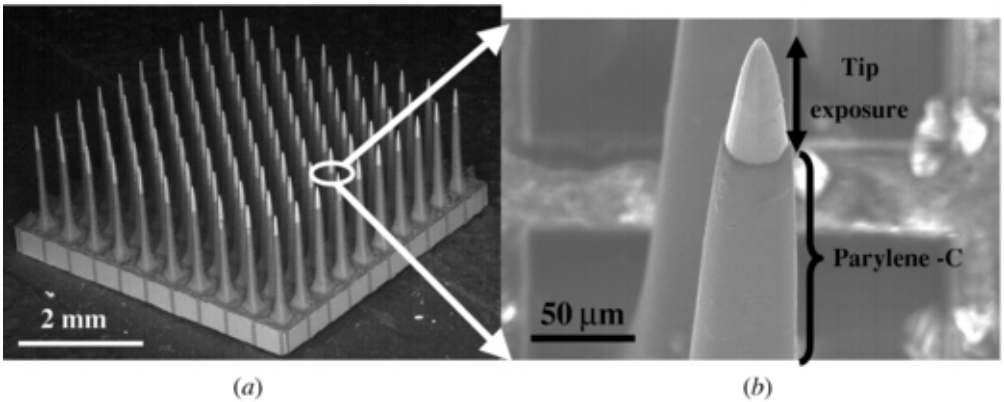

Figure 1.1: Utah microelectrode array. a) Shows a scanning electron microscrope (SEM) image of a 4×4 mm array of 100 electrodes. b) is a high-magnification view of a single electrode tip. Image reproduced with permission from [Negi et al., 2010].

has been used in nearly all human intracortical BCI studies to date. The BrainGate team also demonstrated basic robotic arm control [Hochberg et al., 2012], but this was soon followed by the achievement of continuous BCI control of a robot arm by a tetraplegic subject with seven [Collinger et al., 2013], and then ten [Wodlinger et al., 2014], simultaneously decoded degrees-of-freedom at the University of Pittsburgh.

A number of achievements have been made in recent years, including the addition of functional electrical stimulation (FES) to BCI systems to directly stimulate the user's muscles, restoring hand [Bouton et al., 2016] and arm [Ajiboye et al., 2017] control, and increasingly high-performance communication BCIs with self-calibrating decoders [Jarosiewicz et al., 2015, Pandarinath et al., 2017]. However, all of these systems have relied exclusively on visual feedback. Able-bodied people rely heavily on somatosensation, and it has long been suggested that BCI performance and usability will improve with the addition of sensory feedback (e.g. [Abbott, 2006, Bensmaia and Miller, 2014, Lebedev and Nicolelis, 2006, Mussa-Ivaldi, 2003, Weber et al., 2012]).

1.2 SOMATOSENSORY FEEDBACK

The "sense of touch," or somatosensation, is actually a collection of several sensory modalities, which allow us to detect many qualities associated with object interaction such as pressure, vibration, texture, temperature, and wetness. The somatosensory system can be classified by three functions, exteroceptive (perception of external stimuli), interoceptive (perception of internal stimuli), and proprioceptive (perception of body position) [Abraira and Ginty, 2013]. Four recognized submodalities in the cutaneous somatosensory system include the tactile, thermal, pain, and itch senses [McGlone and Reilly, 2010]. The tactile submodality can be further subdivided into modalities such as perceptions of shape and texture, motion, skin stretch, and vibration, which depend on several types of both rapidly adapting and slowly adapting afferents. These peripheral afferents synapse in the cuneate nucleus of the brainstem and the ventroposterior lateral (VPL) nucleus of the thalamus before projecting to primary somatosensory cortex (S1) [Saal and Bensmaia, 2014], as illustrated in Figure 1.2. Somatosensory feedback, and in particular the tactile and proprioceptive senses, are necessary for fine motor control. A number of case studies have demonstrated the impairments that occur with partial or complete loss of peripheral sensation.

Deafferented patients have exhibited a number of impairments due to their loss of peripheral somatosensation, including the inability to perform dexterous tasks such as buttoning up their clothing or properly manipulating a pen. Such patients tend to grip objects with excessive force in an attempt to avoid accidentally dropping them [Rothwell et al., 1982]. Without proprioception, people make errors in both the planning and execution of movement plans, although visual feedback can be used to make corrections [Gordon et al., 1995]. It is not uncommon for such patients to require a wheelchair due to difficulty balancing, and even with visual feedback, one patient reportedly performed 3–12 standard deviations below normal for various tasks in a test of hand function [Forget and Lamarre, 1987]. These impairments are not solely due to a loss of proprioception, as experiments in which local anesthesia is applied to the fingers have demonstrated that a lack of cutaneous tactile input impairs the ability to handle and manipulate objects [Johansson and Flanagan, 2009, Monzee et al., 2003].

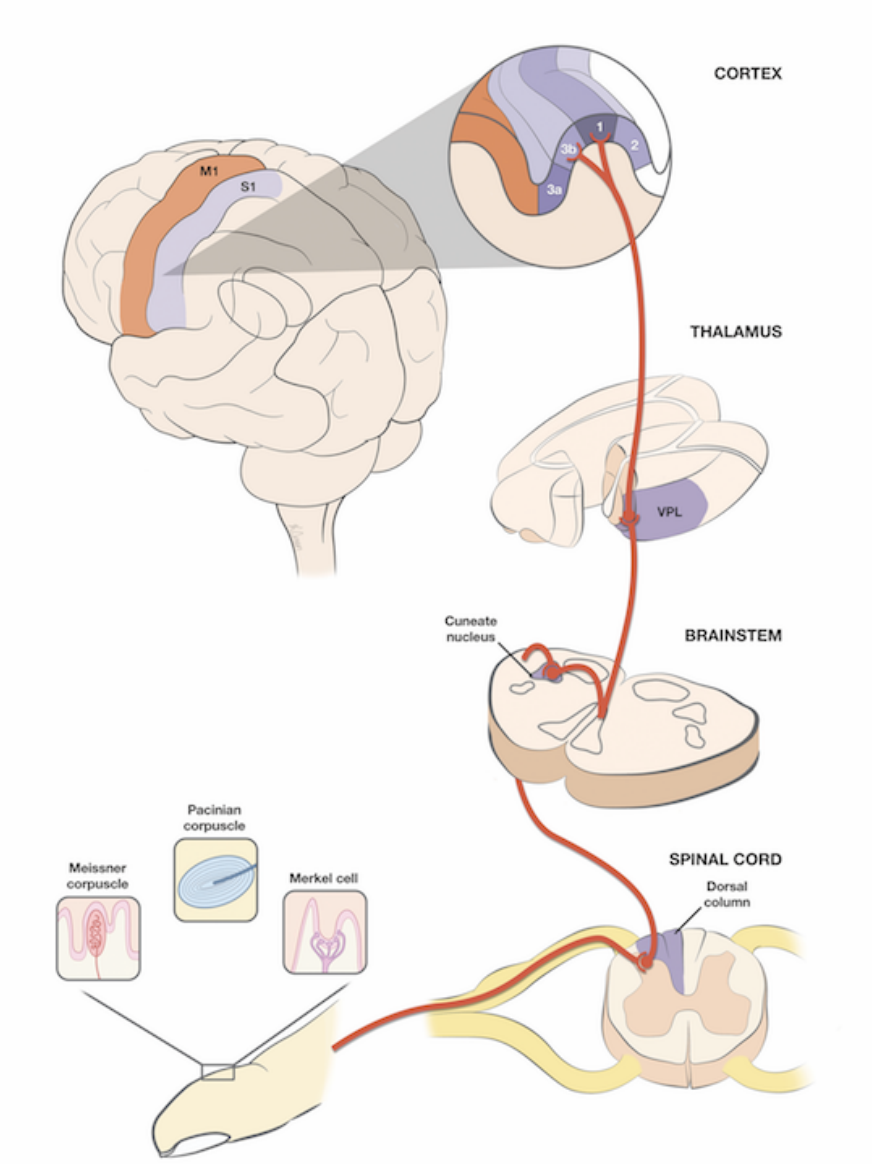

Figure 1.2: Anatomy of the cutaneous tactile somatosensory system. Mechanoreceptors in the skin transduce sensory information into afferent signals that propagate through the spinal cord to the cuneate nucleus and thalamus before synapsing in primary somatosensory cortex. Image credit: Kenzie Green.

While BCIs have enabled paralyzed users to control robotic arms [Collinger et al., 2013, Wodlinger et al., 2014] or even their own hands and arms in conjunction with an FES system [Bouton et al., 2016, Ajiboye et al., 2017], these systems have only provided visual feedback. One can thus draw parallels between BCI arm control and deafferented patients, and expect an upper limit for BCI performance under visual feedback. While limb state can be estimated visually without proprioception, the absence of tactile feedback is particularly likely to impair skillful object manipulation. This problem is not unique to BCI; most prosthetic limbs, particularly those that are myoelectric-controlled, provide limited or no somatosensory feedback [Shannon, 1979]. The need for somatosensory feedback in prosthetic limbs has been stated as early as 1951 [Wiener, 1951], and researchers have experimented with various methods of incorporating artificial sensory feedback into prosthetic limbs for decades.

By the late 1960s and 1970s, several researchers began evaluating the feasibility of using sensorized prosthetics and surface electrical stimulation [Beeker et al., 1967, Rohland, 1975, Shannon, 1979], vibrotactors [Alles, 1970, Carruthers and Pottinger, 1968], or even implanted electrodes [Clippinger, 1973] and intraneural stimulation [Anani et al., 1977, Reswick et al., 1975], to transduce feedback about grip pressure or limb state to the prosthesis wearer. Despite such advances and continued research over many decades (e.g. [D'Anna et al., 2017, D'Anna et al., 2018, Davis et al., 2016, Dhillon and Horch, 2005, Marasco et al., 2011, Raspopovic et al., 2014, Schiefer et al., 2016, Tan et al., 2014]), as well as a preference for better sensory feedback or less reliance on vision by amputees [Atkins et al., 1996, Biddiss and Chau, 2007], artificial sensory feedback is still absent from clinically available prosthetic limbs [Antfolk et al., 2013, D'Anna et al., 2017]. We are interested in restoring somatosensory feedback for BCI users by stimulating in area 1 of primary somatosensory cortex, which is on the surface of the postcentral gyrus in humans and receives input from tactile afferents.

1.3 INTRACORTICAL MICROSTIMULATION

There is a long history of electrically stimulating the nervous system, dating back to early experiments in 1791 by Luigi Galvani that first proposed the role of "animal electricity" as a mechanism for nerves to generate muscle contraction in frogs [Piccolino, 1998], and a self-experiment in the early 1800s by Alessandro Volta documenting a crude procedure for electrically stimulating his own auditory system, generating a sound described as "a kind of crackling, jerking, or bubbling as if some dough or thick material was boiling" [Eshraghi et al., 2012]. In 1870, Fritsch and Hitzig were the first to apply direct electrical stimulation to mammalian cortex and, according to Wilder Penfield, discovered that activation of the frontal cortex generated contralateral movements [Penfield and Boldrey, 1937, Penfield and Rasmussen, 1950]. In 1909, Harvey Cushing first demonstrated that sensations could be generated by electrically stimulating the human postcentral gyrus [Cushing, 1909], and several decades later Wilder Penfield used electrical stimulation to map the surface of human cortex during neurosurgery, leading to the discovery of the motor and sensory cortical homunculus [Penfield and Boldrey, 1937, Penfield and Rasmussen, 1950].

The advent of penetrating microelectrodes in the mid-twentieth century (e.g. [Hubel, 1957, Renshaw et al., 1940]) eventually led to the use of microstimulation to activate small regions of neural tissue by applying small currents in close proximity to neurons. Intracortical microstimulation (ICMS) was first used by Hiroshi Asanuma to study topography and activation thresholds in the motor cortex of cats [Asanuma and Sakata, 1967, Stoney et al., 1968], and has since been used in numerous experimental and clinical studies.

1.3.1 Mechanism of ICMS

In the 1950s, Hodgkin and Huxley performed a series of experiments with a giant squid axon and developed a series of equations modeling the flow of ionic currents across the cell membrane that generate action potentials [Hodgkin and Huxley, 1952]. The Hodgkin-Huxley model revealed the relationship between the voltage across the neural cell membrane and the permeability of sodium and potassium ions through the membrane, leading to the discovery

of voltage-gated ion channels in neural cell membranes. Voltage-gated sodium channels open when the membrane potential is depolarized past a voltage threshold, allowing a rapid influx of sodium ions, followed by an outflux of potassium ions through voltage-gated potassium channels. The flow of ions permitted by these voltage-gated channels result in the action potential current. Electrical stimulation activates neurons by artificially perturbing the extracellular voltage around the cell to depolarize the cell, opening voltage-gated sodium channels and triggering an action potential. While anodal current will cause cells to be locally hyperpolarized, regions further away from the electrode can depolarize with sufficient current [Ranck, 1981]. This behavior is characterized by Rattay's activating function, as demonstrated in Figure 1.3, from [Rattay, 1987]. In either case, current is a more informative parameter for predicting neural recruitment than electrode voltage, as large, time-varying voltage drops occur at the electrode-tissue interface, resulting in a non-linear and non-time-invariant relationship between electrode-voltage and tissue voltage. [Ranck, 1975, Ranck, 1981].

It is generally understood that microstimulation primarily activates axons, and not cell bodies, in close proximity of the electrode, a finding with evidence from both modelling [Rattay, 1999] and in vivo experimentation [Histed et al., 2009, Histed et al., 2013]. It is often assumed that the relationship between stimulus amplitude and threshold for activation is proportional to the square-distance between the neuron and electrode tip [Tehovnik, 1996], as the depolarizing effect of stimulation is thought to activate a spherical volume of neurons around the electrode tip that is a function of stimulation amplitude. However, Ranck noted in 1975 that this assumption is overly simplistic, as many factors affect what is stimulated by an electrode, including the electrical properties and anatomy of neurons, distance and orientation of neural elements relative to the electrode, tissue resistivities, pattern of current flow between the cathode(s) and anode(s), and current waveform (shape, duration, and magnitude) [Ranck, 1975]. Histed et al. used two-photon calcium imaging to demonstrate that ICMS resulted in a sparse activation of neurons both near and far from the electrode, and increases in amplitude resulted in increased density, but not volume, of activated neurons [Histed et al., 2009]. However, this finding is not necessarily contradictory with the theory of stimulation current-distance relationships, as increases in amplitude may result in larger

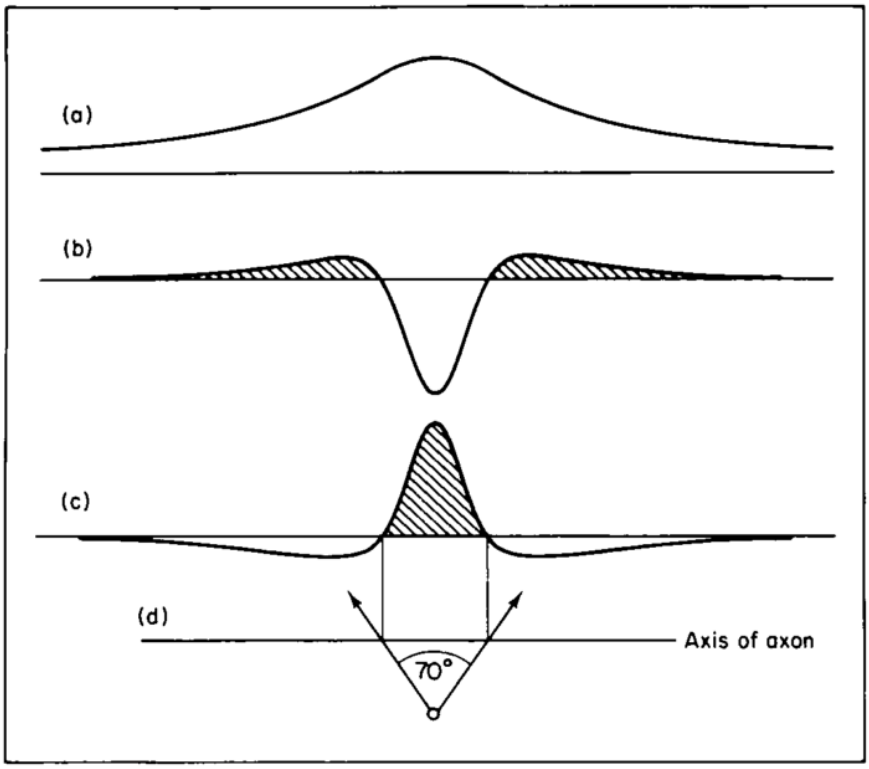

Figure 1.3: Activating function for a non-myelinated axon. (a) Shows the change in extracellular voltage in response to monopolar anodal stimulation, while the activating function for anodal stimulation is shown in (b). The equivalent function for cathodal stimulation is shown in (c). Shaded regions indicate axon segments that are depolarized, and white regions are hyperpolarized. (d) indicates the electrode position and the 70° angle between depolarized and hyperpolarized regions. Figure reproduced with permission from [Rattay, 1987].

spheres of activated axons, resulting in antidromic action potentials activating cell bodies widely distributed around the electrode.

1.3.2 Effects of ICMS on behavior

The effect of ICMS on perception has been difficult to study in animal models, because we cannot simply ask an animal what they feel. Regardless, a number of studies have demonstrated that microstimulation can bias behavior and animals can consciously detect and react to microstimulation.

In 1965, Robert Doty showed that monkeys could be trained to press a lever in response to stimulation from depth electrodes with diameters ranging from 160–250 μm [Doty, 1965]. In 1980, John Bartlett and Robert Doty extended this work, demonstrating that monkeys could be trained to detect and respond to microstimulation in striate cortex with currents as low as 2–4 μA [Bartlett and Doty, 1980]. These experiments required training for the monkey to respond to the stimulus, and thus it is difficult to make inferences about what the monkeys perceived in response to cortical stimulation. Later experiments attempted to address this limitation by introducing ICMS in tasks without explicitly training monkeys to respond to microstimulation.

In 1990, Daniel Salzman, Ken Britten and Bill Newsome demonstrated that microstimulation in visual area MT biased the perception of motion direction in monkeys trained on a motion direction discrimination task [Salzman et al., 1990]. Several years later, Ranulfo Romo demonstrated that monkeys could respond directly to ICMS of primary somatosensory cortex by training monkeys in a flutter frequency discrimination task. When the second mechanical stimulus was replaced with ICMS in area 3b of S1, monkeys could correctly discriminate between the frequencies of mechanical and intracortical stimulation [Romo et al., 1998], and the monkeys could continue performing the task if both stimuli were replaced with ICMS trains [Romo et al., 2000]. A similar experimental design was used to test the behavior of rats in response to ICMS of primary auditory cortex in a frequency discrimination task. Much like Romo's result, the rats were able to discriminate ICMS trains interleaved with auditory stimuli without additional training, and the ICMS responses were similar to those

of auditory stimuli with the preferred frequency of neurons near the electrode [Otto et al., 2005a, Otto et al., 2005b]. While results of animal experiments suggest that ICMS stimuli are nearly indistinguishable from natural stimuli, it is impossible to ask animals what they perceive in response to ICMS. Human studies are required to fully understand the sensations evoked by ICMS.

ICMS was first tested in humans in the 1990s, in an attempt to develop a visual prosthesis. In 1990, Martin Bak et al. tested the use of ICMS in human visual cortex to generate phosphenes in three epileptic patients [Bak et al., 1990]. This study was followed-up by chronically implanting 38 microelectrodes in a blind woman for 4 months [Schmidt et al., 1996]. Phosphenes were reliably generated throughout the 4-month period with detection thresholds as low as 1.9 μA and brightness was modulated by amplitude, frequency, or pulse-width. Furthermore, the phosphenes were more focal than those generated in previous studies ([Brindley and Lewin, 1968, Dobelle et al., 1974]) using macroelectrodes on the cortical surface.

More recently, there has been much interest in using ICMS to provide somatosensory feedback for brain-computer interface control. Nathan Fitzsimmons demonstrated that monkeys could be cued to make reaches based on the spatiotemporal pattern of microstimulation in S1 [Fitzsimmons et al., 2007]. However, unlike Romo's experiment the monkeys required training to perform this task. In a similar experiment, Brian London trained monkeys to perform a two-target reach task and demonstrated that monkeys could distinguish between two frequencies of ICMS in area 3a of S1 used to cue the target direction [London et al., 2008]. Joseph O'Doherty later adapted this task to BCI, and demonstrated that ICMS detection could be used to discriminate between two targets in a BCI-cursor task, although this also required explicit training for the monkey to be successful [O'Doherty et al., 2009]. In a follow-up experiment, O'Doherty also demonstrated that monkeys could be trained to interpret ICMS of S1 as feedback that the cursor was in the target region, rather than as a cue for target direction, and discriminate between frequencies [O'Doherty et al., 2011]. A comparable experiment was repeated by Christian Klaes, in which a monkey was trained to discriminate between two targets using a virtual arm controlled by modulating multi-unit activity in posterior parietal cortex (PPC) [Klaes et al., 2014].

While each of these experiments demonstrated that a closed-loop BCI is possible, the sensory components of the tasks primarily required detection of the stimulation. Maria Dadarlat, Joseph O'Doherty, and Philip Sabes later demonstrated that with significant training, monkeys could learn to interpret multi-channel microstimulation continuously encoding a movement vector as feedback to complete reaches to a target [Dadarlat et al., 2014]. While the authors made no attempt to provide naturalistic percepts, they did demonstrate that ICMS could be used as a continuous feedback source to complete motor tasks. Sliman Bensmaia's group used an experimental design similar to that of [Romo et al., 2000] to show that monkeys trained to perform pressure and location discrimination tasks with mechanical stimuli could continue performing the task in response to ICMS of areas 1 and 3b of S1, without any additional training [Tabot et al., 2013]. Furthermore, they tested the use of a sensory prosthetic by applying mechanical stimuli to a sensorized robotic finger, and mapped sensor data to ICMS pulse trains. Monkeys were able to continue performing the discrimination tasks when stimuli were applied to the robotic finger.

These studies suggest that ICMS is a promising method for developing a sensory prosthetic in visual, auditory, or somatosensory cortex. In a study immediately preceding the work presented in this thesis, Sharlene Flesher et al. demonstrated that ICMS of human primary somatosensory cortex can produce focal, graded tactile percepts, suggesting that ICMS can be used to provide artificial somatosensory feedback as part of a closed-loop neuroprosthetic [Flesher et al., 2016].

1.3.3 Safety of ICMS

In order for ICMS to be feasible for use in a sensory prosthetic, chronic microstimulation must be safe and not result in tissue or electrode damage. Stimulation has the potential to permanently damage neural tissue, evident by the fact that electrolytic lesions have been used for many years as a method of destroying regions of the brain to study the impact on behavior [Horsley and Clarke, 1908, Sweet and Mark, 1953] (typically with larger DC currents of at least 1 mA) or to mark electrode locations [Asanuma, 1981, Hubel, 1959] with sustained DC currents as low as 5 μA. Hiroshi Asanuma noted in 1975 that monophasic

pulse trains began producing noxious effects at 40 μA, and currents of 60 μA resulted in bubbling at the electrode tip and observable tissue damage [Asanuma, 1981].

In 1977, John Bartlett investigated the safety of ICMS and determined that neuronal damage occurs due to electrode polarization and hydrolysis, and detection thresholds increased when electrodes were not discharged between pulses [Tehovnik, 1996]. Brummer and Turner had previously presented an overview in 1975 of the electrochemical reactions that occur when stimulating through a platinum microelectrode, including the irreversible hydrolysis reaction that occurs with sufficiently high voltage, releasing oxygen and hydrogen gas from water, and changing local pH by generating hydrogen ions [Doty and Bartlett, 1981]. In Bartlett's study, neural damage and threshold increases were avoided by using charge-balanced biphasic pulses to avoid polarizing the electrode [Tehovnik, 1996], a method first used in 1955 and originally termed the "Lilly" waveform [Doty and Bartlett, 1981]. This method can keep the tissue-electrode interface within the "water window," the potential range in which hydrolysis of water does not occur [Merrill et al., 2005].

Using larger electrodes, Vernon Rowland had previously found in 1960 that charge-balanced pulses with less than 20,000 nC/phase did not produce lesions in cat cortex, but pulses with greater than 25,000 nC/phase generated lesions with sizes linearly proportional to charge per phase, and not related to frequency or waveform shape (including interphase period) [Tehovnik, 1996]. In fact, tissue damage in response to stimulation is explained by an interaction between charge density and charge per phase [McCreery et al., 1990]. Charge density increases with reduced electrode size, and thus microelectrodes can cause damage with much lower levels of charge [Tehovnik, 1996]. More recently, sputtered iridium oxide film (SIROF) microelectrodes have been developed that are capable of delivering current with lower voltages than electrodes made of high-impedance materials such as platinum [Negi et al., 2010], and can be reliably used for chronic microstimulation without exceeding water window limits or degrading recording quality [Kane et al., 2013, Torab et al., 2011]. In a nonhuman primate study designed to evaluate safe ICMS procedures for the human work conducted by our lab and presented in this thesis, Alexander Rajan et al. demonstrated that chronic ICMS, with biphasic pulses of up to 100 μA at 300 Hz with a 50% duty cycle (5 seconds on:5 seconds off), and delivered through SIROF microelectrode arrays, did not

impair motor control or result in tissue damage beyond what would be expected for a non-stimulated array [Rajan et al., 2015]. The work presented in this thesis was subject to safety limits based on this study. Biphasic pulses were limited to 100 μA in amplitude and could not be stimulated for more than 1500 pulses within a 30 second window (based on a 50% duty cycle at 100 Hz). A complete list of safety parameters is presented in Appendix B.

1.3.4 Stimulation artifacts

Despite the small currents used for microstimulation, large voltages are generated due to the relatively high impedance of microelectrodes and the electrode-tissue interface. These large voltages present as large artifacts in microelectrode recordings that are several orders of magnitude larger than extracellular spike potentials (See Figure 2.4). Stimulation artifacts mask spikes, often saturate recording amplifiers, and can last longer than the actual stimulus pulse. Artifacts have been noted as an obstacle to simultaneous recording and stimulation since the earliest days of ICMS [Stoney et al., 1968], and a variety of methods have been presented in an attempt to reduce the impact of artifacts with varying degrees of success.

Stimulation artifacts appear in recordings due to conduction of the stimulus current through tissue, and capacitive crosstalk between stimulating and recording leads [Wagenaar and Potter, 2002, Grumet, 1999]. Furthermore, high-gain amplifiers are likely to saturate in response to stimulation, producing nonlinear output. Amplifiers also typically include bandpass filters for noise reduction and anti-aliasing. Both saturation and filtering can extend the artifact duration, in some cases up to 100 ms [Wagenaar and Potter, 2002].

Electrode geometry can have a notable impact on the severity of stimulus artifacts, and bipolar stimulation has often been used in an attempt to reduce artifacts [Ranck, 1981]. However, bipolar stimulation is less understood and may not follow the current-distance relationships of monopolar stimulation. Depending on electrode and fiber geometry, axons may be oriented orthogonally to the voltage gradient and fail to activate, or a fiber depolarized and activated by a cathode may be hyperpolarized by the anode, blocking the action potential from propagation [Ranck, 1975, Ranck, 1981]. Many techniques have been proposed to reduce or eliminate artifacts during monopolar stimulation, such as sample-and-hold

[Freeman, 1971] or template subtraction [Limnuson et al., 2014, McGill et al., 1982], but all methods have unique limitations and issues with generalizability. Our goals necessitate a robust method to record spikes and reject artifacts in real-time while applying monophasic ICMS in an adjacent area of cortex, without making significant changes to existing hardware, which has been cleared for human use by the U.S. Food and Drug Administration (FDA). Additional background on stimulation artifacts is presented in Chapter 2, followed by my solution to the problem.

1.4 RESPONSE LATENCY OF SENSORY FEEDBACK

In order for artificial sensory feedback in a prosthetic and brain-computer interface to be useful, the user must be able to interpret and make use of encoded information in a timely manner. For example, if a prosthetic user begins to apply excessive force on a breakable object such as an egg, the user must receive feedback quickly enough to react and loosen their grip before breaking the object. Alternatively, if an object begins to slip out of their hand, the user must increase grip force before the object is dropped. Vision is not necessarily perceived quickly enough to correct for such perturbations, as deafferented patients struggle to maintain a stable grasp even while observing their hand [Rothwell et al., 1982].

The need for a fast rate of information transfer in feedback for prosthetics was identified many decades ago (e.g. [Carruthers and Pottinger, 1968]), but there has been limited work investigating the timing criteria that must be met for a feedback method to be useful. In addition to the need for providing useful information in a timely manner in order to improve *performance*, evidence suggests that feedback must be delivered quickly to facilitate *embodiment* [Tabot et al., 2015]. The rubber hand illusion is a phenomenon that occurs when a person receives tactile stimulation on their unseen hand while simultaneously observing stimulation applied to a rubber hand. If the visual and tactile stimuli are applied simultaneously, the person is likely to feel as though the rubber hand is part of their own body, but the illusion typically fails if the tactile stimulation is delayed with respect to the visual stimulation by more than 300 ms [Shimada et al., 2009].

Sensory feedback is often used in unconscious mechanisms such as reflexes. While cortical stimulation cannot replicate the reflexes that occur in the spinal cord or brainstem, there may be long-loop reflex circuits in cortex that could potentially be influenced by stimulation [Weber et al., 2012]. For example, cutaneous feedback has been shown to contribute to reflex-like activity in motor cortex in response to object slip perturbations [Picard and Smith, 1992]. While the unconscious use of feedback should be a goal for sensory prosthetics [Antfolk et al., 2013], it is likely that feedback will need to be consciously perceived and evaluated to inform a change in motor plan, and these events must happen quickly in order to respond to perturbations.

While we might expect response times to ICMS, which bypasses conduction through afferent circuits, to be faster than responses to peripheral stimuli, there are conflicting reports on the response times to ICMS. Ranulfo Romo noted that monkeys receiving ICMS in area 3b of somatosensory cortex exhibited reaction times that were indistinguishable from mechanical stimuli in a discrimination task [Romo et al., 2000]. Kevin Otto found that response latency to ICMS of auditory cortex in rats was significantly faster than to auditory stimuli in a similar discrimination task [Otto et al., 2005a, Otto et al., 2005b]. On the other hand, slow reaction times to ICMS were documented in a blind human patient implanted with microelectrodes in visual cortex [Schmidt et al., 1996], although the authors noted the known relationship between reaction time and phosphene size and brightness [Kohfeld, 1971].

In an attempt to directly address this issue, Jason Godlove et al. compared the use of visual, vibrotractile, and ICMS cues in a redirect reaching task [Godlove et al., 2014]. The authors were surprised to find that a monkey responded to ICMS slower than to visual or vibrotactile stimulation. The authors had initially hypothesized that response time to ICMS would be faster than to tactile stimulation because directly stimulating the cortex bypasses afferent pathways. For humans, conduction delays from peripheral afferents to second-order neurons in the cuneate nucleus are on the order of 14–28 ms [Antfolk et al., 2013, Johansson and Flanagan, 2009], so one might expect reaction times to cortical stimulation to be faster by a similar margin. The authors suggested several explanations for why they observed slow reaction times, such as the fact that they may have activated cortex with unnatural patterns of activity that needed to be refined and amplified by downstream processing, whereas such

amplification and refinement would normally occur in upstream processes, such as in the thalamus [Godlove et al., 2014]. It is also worth emphasizing that these findings were not repeated in more than one animal.

The conflicting reports of response times to ICMS in the literature motivates my study in Chapter 3, in which my goals are to characterize the reaction times to ICMS of somatosensory cortex for a human participant, and compare against reaction times to visual and peripheral tactile stimuli.

1.5 MOTIVATION AND GOALS FOR CLOSED-LOOP BCI DEVELOPMENT

1.5.1 Current state of field

Prior to the start of the work presented in this thesis, many advancements had been made in the field of BCI, such as ten degree-of-freedom control of a robotic limb by a paralyzed individual [Wodlinger et al., 2014]. However, limited progress had been made to incorporate sensory feedback into such a system, despite the acknowledgement that nonvisual feedback was necessary [Weber et al., 2012]. A number of animal experiments demonstrated that trains of intracortical microstimulation in somatosensory cortex could be detected and discriminated, as summarized in Section 1.3.2, but the use of ICMS in humans was limited to two studies evaluating the feasibility of a visual prosthesis [Bak et al., 1990, Schmidt et al., 1996]. Concurrent with the start of this work, our lab demonstrated for the first time that ICMS of human somatosensory cortex can evoke focal tactile sensations that are graded by amplitude [Flesher et al., 2016]. This was an encouraging result that renewed optimism in the feasibility of a closed-loop BCI system. However, several unknowns remained to be solved.

1.5.2 Elimination of stimulus artifact

A well-known challenge to simultaneously recording and stimulating in cortex is the stimulus artifact that corrupts recordings during and after each stimulus pulse, as described in Section 1.3.4. While many techniques have been described to reduce or eliminate stimulation artifacts, it was unclear if any of these techniques would be applicable to the requirements of our system. Our lab was granted an Investigational Device Exemption by the U.S. Food and Drug Administration (FDA), which required that we use clinically approved, safe hardware without modification. Thus, we needed to implement a robust method for real-time artifact rejection that was compatible with our FDA-cleared hardware. Our design goals were to implement a simple, robust method to record and stimulate in adjacent regions of cortex. We desired a method that was robust to amplifier saturation and allowed for recording as soon as 1 ms after each stimulus pulse. We also wished to avoid substantial changes to our clinical BCI system, particularly hardware modifications that would require additional review by the FDA. Finally, the primary goal was to implement an artifact rejection method effective enough to allow for multi-channel ICMS during BCI control without any degradation in performance. I have implemented such a method by applying two simple modifications to our system, which is described in Chapter 2. Furthermore, I validated the method in Section 2.3.5 by demonstrating that skillful BCI performance is maintained during multi-channel ICMS with artifact rejection in place.

1.5.3 Characterization of ICMS reaction times

A critical unknown is whether the sensations elicited by ICMS can be interpreted and used effectively to improve motor control. This multi-faceted problem is beyond the scope of this thesis, but it can be broken down into smaller components. One critical issue is the latency between stimulus onset and when a user is able to respond to the feedback. This latency is likely task-dependent, but conflicting reports exist in literature, including a study that suggested that response time to ICMS was slower than either visual or vibrotactile stimuli [Godlove et al., 2014]. This finding was troublesome, because if a user cannot perceive and respond to a feedback signal quickly enough, the signal will not be useful for influencing

motor control. I chose to investigate this issue by characterizing the simple reaction time to single-channel ICMS of somatosensory cortex in a human BCI participant, as summarized in Chapter 3. I compared reaction times to ICMS with reaction times to visual stimulation and electrical stimulation on the hand, in both the BCI participant and able-bodied control subjects, and found that ICMS reaction times were similar, and perhaps faster, than reaction times to peripheral stimuli.

1.5.4 Impact and future work

The work presented in this thesis provide evidence in favor of the viability of using ICMS for feedback in closed-loop BCI. ICMS can be used without degrading the performance of BCI decoders, and humans can respond to ICMS with reactions times comparable to peripheral sensory input. This will enable us to study how to effectively transmit sensory information to supplement visual feedback with feedback variables such as object contact and applied force. The use of ICMS feedback will hopefully allow for dexterous object manipulation beyond what is currently possible with state-of-the-art intracortical BCI systems.

2.0 ARTIFACT-FREE RECORDING DURING HUMAN INTRACORTICAL MICROSTIMULATION

The contents of this chapter are in preparation for submission to the Journal of Neural Engineering by: Jeffrey M. Weiss, Sharlene N. Flesher, Robert Franklin, Jennifer L. Collinger, and Robert A. Gaunt.

In this chapter, I describe and validate a simple and robust method for removing stimulation artifact from microelectrode recordings in real-time and using FDA-cleared hardware for use in a closed-loop intracortical brain computer interface.

2.1 INTRODUCTION

A major goal of neuroprosthetic research is to restore motor function to individuals with upper extremity paralysis. Recent work has shown that it is possible to achieve high degree-of-freedom control of a robotic arm using a brain-computer interface (BCI) [Collinger et al., 2013, Wodlinger et al., 2014]. While performing simple object interactions with a BCI-controlled limb has been successful, dexterous control remains a significant challenge. One limitation of current BCI systems is the absence of somatosensory feedback. It is known that humans require somatosensory feedback to perform dexterous object manipulation [Johansson et al., 1992, Monzee et al., 2003], but in general BCI systems only provide visual feedback. We have recently shown that it is possible to generate graded tactile percepts using intracortical microstimulation (ICMS) [Flesher et al., 2016], suggesting that microstimulation has potential as a source of somatosensory feedback in a closed-loop BCI system. Sensors on a BCI-controlled end-effector can be used to modulate stimulus parameters. By

supplementing visual feedback with ICMS tactile feedback, it may be possible to perform dexterous tasks using a BCI that were previously not feasible.

While the concept of incorporating microstimulation into a BCI system is not new [Abbott, 2006, Bensmaia and Miller, 2014, Fitzsimmons et al., 2007, Lebedev and Nicolelis, 2006, Mussa-Ivaldi, 2003, Venkatraman et al., 2009, Weber et al., 2012], progress in this area has been relatively slow. A significant technical hurdle is the ability to record spikes while stimulating in an adjacent brain area. Microstimulation generates voltages orders of magnitude greater than the microvolt-scale extracellular spike potentials produced by neurons. When filtered, these large, brief stimulus pulses can generate artifacts several milliseconds in duration. While the onset timing of primary stimulus artifacts is precisely known, the secondary artifacts occurring after each stimulus pulse are often unpredictable. The long duration and unpredictability of stimulus artifacts present difficulty in reliably masking out artifacts and detecting neural spikes. A closed-loop BCI system must have a robust method for artifact rejection to decode uninterrupted motor commands during ICMS.

A number of artifact rejection solutions have been proposed previously, with varying degrees of simplicity and generalizability. One proposed solution is to alternate recording and stimulus trains in time, e.g. in 50 ms intervals. This method was used to instruct target selection via ICMS in a two-dimensional BCI control task [O'Doherty et al., 2011]. This approach may not be optimal, as only 50% of neural data is preserved and stimulation can only occur in bursts, rather than in a continuous pulse train. A better solution would allow stimulation to occur continuously with minimal neural data loss. Alternative solutions for artifact rejection include more sophisticated signal processing techniques such as various methods of template subtraction or modeling [Klaes et al., 2014, Limnuson et al., 2014, Mena et al., 2017, O'Shea and Shenoy, 2018, Wagenaar and Potter, 2002], regression-based referencing [Young et al., 2018], or a combination of bipolar stimulation with adaptive-filtering [O'Doherty and Sabes, 2016]. Some of these alternative solutions allow spikes to be detected during the stimulus, but only in experiments where the amplifiers are never saturated, and sometimes requiring noncausal processing, resulting in additional challenges to rejecting artifacts in real-time [O'Shea and Shenoy, 2018, Young et al., 2018]. Many of these methods also require a training dataset to generate stimulus artifact templates or

model parameters. We sought a simple, generalizable method for artifact rejection that did not require training and could be implemented in real-time using existing hardware.

This work was conducted as part of a larger brain-computer interface (BCI) study with three main goals: 1) demonstrate high degree-of-freedom BCI arm control in tetraplegic subjects [Collinger et al., 2013, Wodlinger et al., 2014], 2) demonstrate the use of intracortical microsimulation (ICMS) to provide somatosensation in an SCI subject [Flesher et al., 2016], and 3) demonstrate the use of ICMS-provided feedback to improve BCI control. The final goal of closed-loop BCI control necessitates a bidirectional electrophysiology system capable of recording neural activity in motor cortex while simultaneously stimulating in somatosensory cortex. We propose a simple yet robust solution to artifact rejection that minimizes neural data loss while using existing FDA-approved clinical hardware and avoiding complicated signal processing techniques that may fail to generalize.

2.2 METHODS

2.2.1 Array implantation

A 28-year old male participant[1] with spinal cord injury enrolled in the study. The participant sustained a spinal cord injury 10 years prior to implantation and presented with a C5 motor/C6 sensory ASIA B spinal cord injury. Presurgical MEG imaging, as described previously [Flesher et al., 2016], was used to identify the hand areas of primary motor cortex (M1) and area 1 of primary somatosensory cortex (S1). Two cortical recording and stimulating (CRS) microelectrode array systems (Blackrock Microsystems, Salt Lake City, Utah) were implanted in the participant's left cortex, as shown in Figure 2.1. Each CRS array system consisted of an 88-channel platinum Utah array and a 32-channel sputtered iridium oxide film (SIROF) Utah array wired to a Neuroport pedestal connector. The two platinum arrays were implanted in the hand and shoulder areas of left motor cortex, while the two SIROF arrays were implanted in the hand area of left primary somatosensory cortex. The motor cortex arrays were used for recording, while the somatosensory arrays were used for

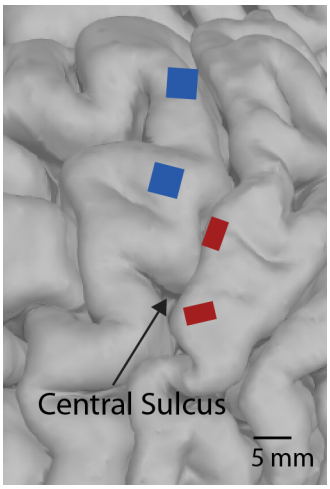

Figure 2.1: Location of implanted electrode arrays marked on pre-surgical anatomical MR image. Blue boxes indicate location of recording (M1) arrays and red boxes indicate location of stimulating (S1) arrays. Array locations were determined by intraoperative photos and postsurgical CT imaging.

intracortical microstimulation. The goals of our study do not necessitate simultaneously stimulating and recording from the same array.

The study was performed under an Investigational Device Exemption granted by the U.S. Food and Drug Administration. The study received approval from the Institutional Review Boards at the University of Pittsburgh and the Space and Naval Warfare Systems Center Pacific and is registered at ClinicalTrials.gov (NCT01894802).

2.2.2 Bidirectional electrophysiology system

Neural recording was accomplished using two Neuroport clinical electrophysiology systems, each consisting of a Neural Signal Processor (NSP) and Front-End Amplifier (Blackrock Microsystems, Salt Lake City, UT). The amplifiers have a sample-and-hold feature, allowing the recordings to be "blanked" during stimulation pulses. A TTL input can gate the amplifier's analog-to-digital converter (ADC), causing it to stop sampling the analog input signal and

[1] In Chapter 3, this subject is referred to as CRS2.

instead hold the last-sampled value on each channel as output. Spike extraction occurs on the Neural Signal Processor by applying a digital high-pass filter and thresholding for spikes.

Intracortical microstimulation (ICMS) was delivered using the Cerestim R96 microstimulator (Blackrock Microsystems). The stimulator's sync output produces a TTL pulse beginning 60 microseconds before each stimulus pulse. A monostable multivibrator (Texas Instruments CD74HC123, Dallas, TX) was used to generate a TTL pulse of an arbitrary duration set by a potentiometer and triggered by the stimulator's sync signal. This TTL pulse was used to blank the recording during stimulation pulses by gating the sample-and-hold feature of the amplifiers. A timing diagram of this process is shown in Figure 2.2.

The Cerestim R96 and Neural Signal Processors interfaced with a BCI software suite written in C++ and Matlab. This software was configured to reject spikes caused by transient threshold crossings at the offset of the sample-and-hold blanking period, as a result of discontinuous sampling of the analog signal. The complete bidirectional electrophysiology system is shown in Figure 2.3.

The system presented above has two primary components that can be tuned to reject stimulation artifacts, while preserving neural data. First, the digital filter used for spike extraction can be tuned to minimize the effect of stimulation artifacts. Second, the raw signals can be blanked during stimulation for an arbitrary duration. This blanking duration can be tuned to balance removing the artifact from the raw signal, while also preserving neural data. These features were tuned using raw voltage recordings collected from electrodes in motor cortex during intracortical microstimulation of somatosensory cortex.

2.2.3 Open-loop recording experiments

Electrode recordings from both M1 arrays were collected during open-loop intracortical microstimulation trials for the purpose of tuning and validating the artifact rejection system. Analog voltage recordings were band-pass filtered (0.3–7500 Hz) and digitized at 30,000 samples per second. Signal blanking and digital filters were not applied online. This allowed for the artifact rejection and spike detection features to be implemented and tuned offline on the raw, artifact-contaminated signals.

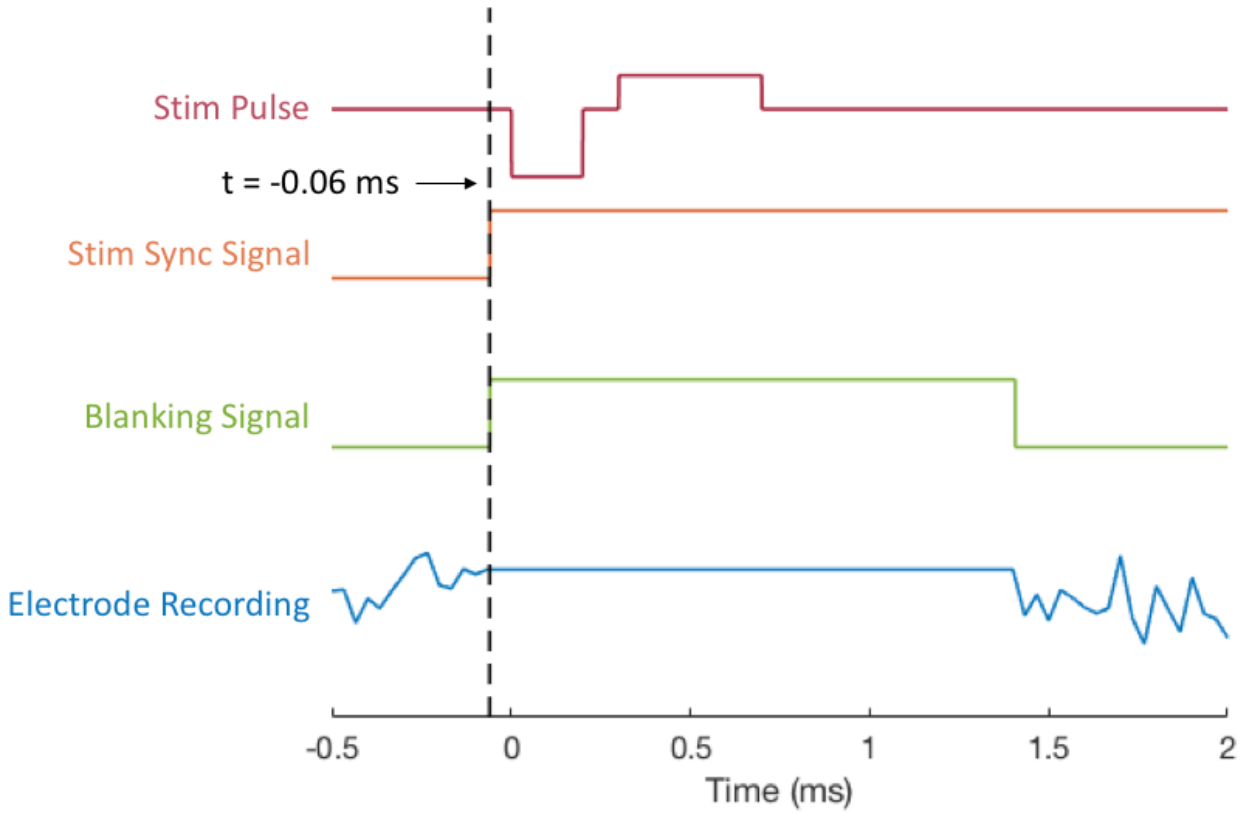

Figure 2.2: Signal blanking timing diagram. Each biphasic stimulus pulse consisted of a 0.2 ms cathodal period, followed by a 0.1 ms interphase period and a 0.4 ms anodal period. The stimulator outputs a TTL sync signal beginning 0.06 ms before the stimulus pulse and ending at $1000/F$ ms, where F is the commanded stimulation frequency. The rising edge of the sync signal triggered the blanking circuit to output a TTL blanking signal of a fixed, experimenter-defined duration. This blanking signal triggered the amplifier's sample-and-hold feature, resulting in each electrode recording to maintain a constant value from 0.06 ms prior to the stimulus pulse until the falling edge of the blanking signal.

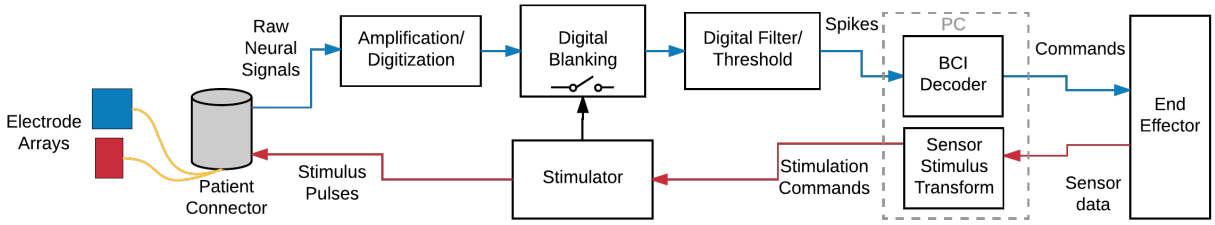

Figure 2.3: Closed-loop system diagram. Each recording array (blue) records neural signals, which are digitized, filtered, and decoded to control an end effector. Sensor data from the end effector are transformed to generate stimulation commands, which are delivered through the stimulating arrays (red). The recording signal is blanked during stimulus pulses to remove the majority of the artifact before filtering.

Intracortical microstimulation consisted of trains of charge-balanced, cathodic-leading asynchronous pulses delivered at 100 Hz. Each pulse had a 200 μs cathodal phase, 100 μs interphase, and 400 μs anodal phase. Cathodal amplitudes ranged from 2–100 μA; anodal amplitudes were always half of the cathodal amplitude. Up to twelve electrodes could be simultaneously stimulated, with a maximum total charge per phase of 144 nC.

2.2.4 Digital filter analysis

Digital filters affect both artifacts caused by ICMS as well as the neural spike signal of interest. In a typical neural recording setup, a digital fourth-order Butterworth filter with a high-pass cutoff frequency of 250–300 Hz is used to remove low frequency components of the recorded signal [Fraser et al., 2009, Simeral et al., 2011]. To study the effects of cut-off frequency on the ability to record spikes, the band-pass filter analysis from [Lempka et al., 2011] was replicated on data recorded from M1 in the absence of stimulation. Raw voltage signals were initially filtered with a fourth-order high-pass Butterworth filter with a 250 Hz cutoff frequency, as in [Collinger et al., 2013], and thresholded at -4.5 times the root-mean-square standard deviation to extract spike snippets. The spike snippets were then

sorted and spike times were saved for each single-unit. The raw voltage signals were then re-filtered with a second-order band-pass Butterworth filter with varying cutoff frequencies, as in [Lempka et al., 2011], and sorted snippets were extracted using the previously determined spike times. The mean peak-to-peak voltage, noise estimate, and signal-to-noise ratio (SNR) was calculated for each unit and filter setting. The noise estimate was calculated as the standard deviation of the first five samples of each snippet, which is prior to the start of a typical action potential. The SNR was calculated as the mean peak-to-peak voltage divided by two times the noise estimate. This analysis was then repeated with first-order high-pass Butterworth filters.

2.2.5 Closed-loop BCI system

The bidirectional electrophysiology system described in Section 2.2.3 was used to develop a closed-loop BCI system, expanding on the high degree-of-freedom BCI system presented previously [Collinger et al., 2013, Wodlinger et al., 2014].

2.2.5.1 Decoding The filtered spike signal described above was thresholded at -4.5 times the root-mean-square (RMS) voltage value to detect spikes. Digital filters and thresholds were applied in real-time on the Neural Signal Processors (Blackrock Microsystems). No spike sorting was applied; threshold crossings on each recording channel were treated as a single-unit. Firing rates were estimated using 20 ms bins of spike counts, which were then smoothed using an exponential function with a 440 ms sliding window. The two-phase calibration procedure previously described [Collinger et al., 2013] was used to train an optimal linear estimator (OLE) decoder to control the Modular Prosthetic Limb (Johns Hopkins University Applied Physics Lab). The resulting decoder predicts endpoint and grasp velocity by relating the firing rate, f, of each unit to five-dimensional velocity, v, using equation 2.1.

$$f = b_0 + b_x v_x + b_y v_y + b_z v_z + b_r v_r + b_g v_g \tag{2.1}$$

The five-dimensional velocity includes x, y, and z endpoint translation components, an endpoint roll orientation component, r, and a grasp component, g. Optimal linear estimation

with ridge regression was used to determine decoding weights from each b coefficient to predict arm kinematics from the recorded firing rates. During testing, firing rates were scaled using equation 2.2 prior to decoding to account for global changes in firing rate [Downey et al., 2017]. Firing rates were multiplied by the mean firing rate during training divided by the mean firing rate over the previous 300 ms.

$$f_{\text{scaled}} = f \cdot \frac{\text{mean}(f_{\text{training}})}{\text{mean}(f_{300\text{ ms}})} \tag{2.2}$$

2.2.5.2 Sensor-stimulus transform To generate stimulus commands, torque sensors on the digits of the Modular Prosthetic Limb were mapped to electrodes in S1, as previously described [Flesher et al., 2016]. Torque sensor values, T, were linearly converted to stimulation amplitude, A, using equation 2.3, such that electrodes began stimulating at a minimum amplitude, A_{min}, when the corresponding sensor value crossed a defined threshold, T_{min}, and increased linearly in amplitude with increasing torque until a maximum value, A_{max}, was reached at a defined maximum torque value, T_{max}. Stimulus frequency was fixed at 100 Hz. Stimulus pulses were charge-balanced and asymmetric, with a 200 μs cathodic phase, followed by a 100 μs interphase period and a 400 μs anodic phase.

$$A = \left(\frac{T - T_{\text{min}}}{T_{\text{max}} - T_{\text{min}}}\right)(A_{\text{max}} - A_{\text{min}}) + A_{\text{min}} \; ; \; T_{\text{min}} \leq T \leq T_{\text{max}} \tag{2.3}$$

2.2.6 Object transfer task

The closed-loop system was evaluated using an object transfer task. The goal of this experiment was to demonstrate that the artifact rejection features enable closed-loop BCI performance that is functionally equivalent to BCI performance without stimulation. In each session, a five DOF velocity decoder was trained as described in Section 2.2.5.1. The decoder's functional performance was then evaluated with an object transfer task, in which the subject was required to use the Modular Prosthetic Limb to grasp a cylinder on the left side of a table, pick it up, and transfer it to the right side of the table. A 20 cm wide region in the center of the table was indicated by two lines of tape. The subject was required to

hold the object above this region while transporting it, rather than simply drag the object across the surface of the table. If the object contacted the table at any point in this region, the subject was required to bring the object back to the left to reset the transfer. The task was scored based on the number of successful transfers in two minutes. On a given day of testing, the system was configured with either a fourth-order Butterworth 250 Hz high-pass spike filter, as used in previous studies, or a first-order Butterworth 750 Hz high-pass spike filter. Filter settings and thresholds were fixed throughout each testing day. Within each day, three task conditions were tested in a block design: no stimulation, stimulation with artifact rejection, and stimulation without artifact rejection. Here, artifact rejection refers to signal blanking and software rejection. In all cases, coincidence detection, a standard feature of the Neural Signal Processor, was enabled to reject threshold crossings that occurred simultaneously on at least 45 channels. During task conditions with stimulation, eight electrodes spanning both S1 stimulation arrays were mapped to the index finger torque sensor and simultaneously amplitude-modulated using the sensor-stimulus transform in Equation 2.3.

2.3 RESULTS

2.3.1 Recordings during ICMS

The stimulation artifacts recorded in primary motor cortex during microstimulation of primary somatosensory cortex were typically on the scale of millivolts, and often saturated the amplifier when exceeding eight millivolts. These artifacts were 1–2 orders of magnitude larger than most extracellular potentials, such as those in Figure 2.4. Even in the case of amplifier saturation, spikes were often observed in the raw voltage signal within one millisecond of the offset of microstimulation. Therefore, we determined that it would be possible to discard artifacts and recover spikes a short duration after each stimulus pulse. Our artifact rejection scheme is the result of applying a minimal number of changes to our existing clinical BCI system. Signal-blanking duration and digital filter parameters were tuned to allow us to reliably record artifact-free spikes between each stimulation pulse.

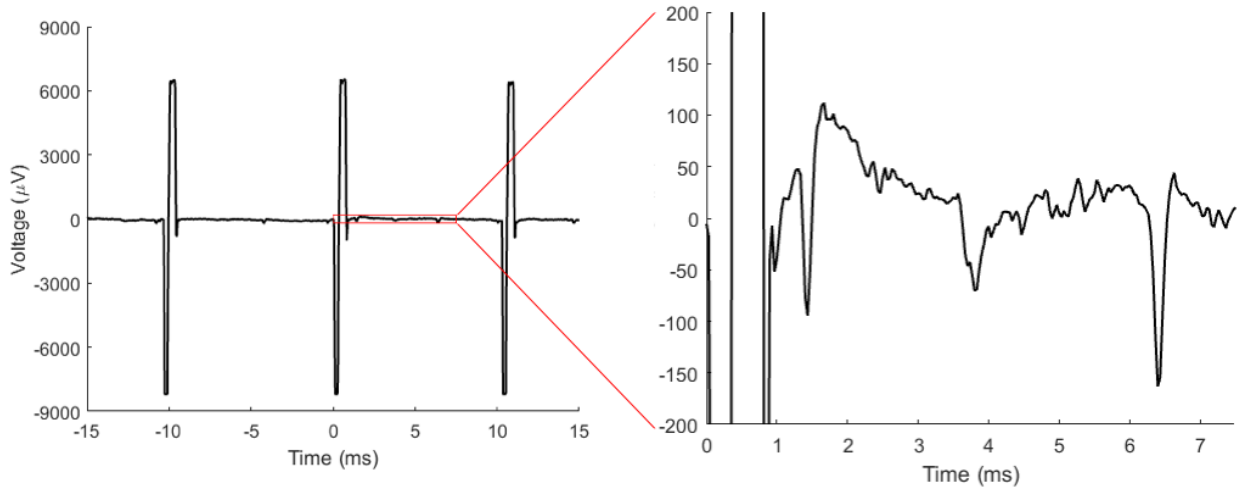

Figure 2.4: Example recording during microstimulation. Stimulation artifacts are several orders of magnitude larger than extracellular spike recordings and often saturate the amplifier. (left) Three stimulation artifacts are shown, along with several neural spikes. Each artifact saturates the amplifier during the cathodal phase. (right) Detailed view of the red boxed region on the left. Spikes can be seen at approximate times 1.3, 3.5, and 6.2 ms. The first spike begins approximately 0.6 ms after the offset of stimulation.

2.3.2 Digital spike filters

A typical neural recording scheme involves recording a high bandwidth voltage signal (i.e. 0.3–7500 Hz bandpass-filtered signal sampled at 30,000 samples per second), applying a digital spike filter, and then applying a voltage threshold on the filtered signal to detect spikes. A good spike filter is typically designed to filter out low-frequency local field potentials (LFPs) while passing high-frequency action potentials that can be detected via thresholding. For example, in previous studies we used a fourth-order Butterworth high-pass filter with a 250 Hz cutoff frequency [Collinger et al., 2013, Wodlinger et al., 2014]. However, ICMS introduces another source of high-frequency content that can lead to undesirable filter output. We wanted to explore how modified filters alone could reduce the effect of the ICMS artifact.

Microstimulation generates high-amplitude primary stimulus artifacts that are impulse-like in nature. These high-amplitude artifacts generate filter output approximating the filter's impulse response, distorting the artifact. For infinite impulse response (IIR) filters, this can cause ringing in the filter output, often resulting in spurious threshold crossings, or secondary artifacts, long after the initial stimulus artifact.

In many signal-processing applications, filter parameters are chosen to best approximate an ideal filter in the frequency domain. For this reason, higher-order Butterworth filters are often preferred for their short transition bands and flat passbands and stopbands. In our case, we determined that the time domain properties of the filter were more critical than the frequency domain properties because we wish to detect spikes as quickly as possible after each stimulation pulse. The secondary artifacts due to filter ringing can be reduced or eliminated by choosing a filter with an impulse response exhibiting a fast settling time and few or no oscillations. The impulse responses to several high-pass Butterworth filter designs are shown in Figure 2.5. We chose a first-order filter design to eliminate oscillations in the impulse response. High-pass Butterworth filters with increased cutoff frequencies feature impulse responses with faster settling times. Therefore, we used a higher cutoff frequency than in previous studies.

The effects of fourth-order, 250 Hz and first-order, 750 Hz high-pass Butterworth filters on an example stimulus artifact are demonstrated in Figure 2.6. Our final spike filter im-

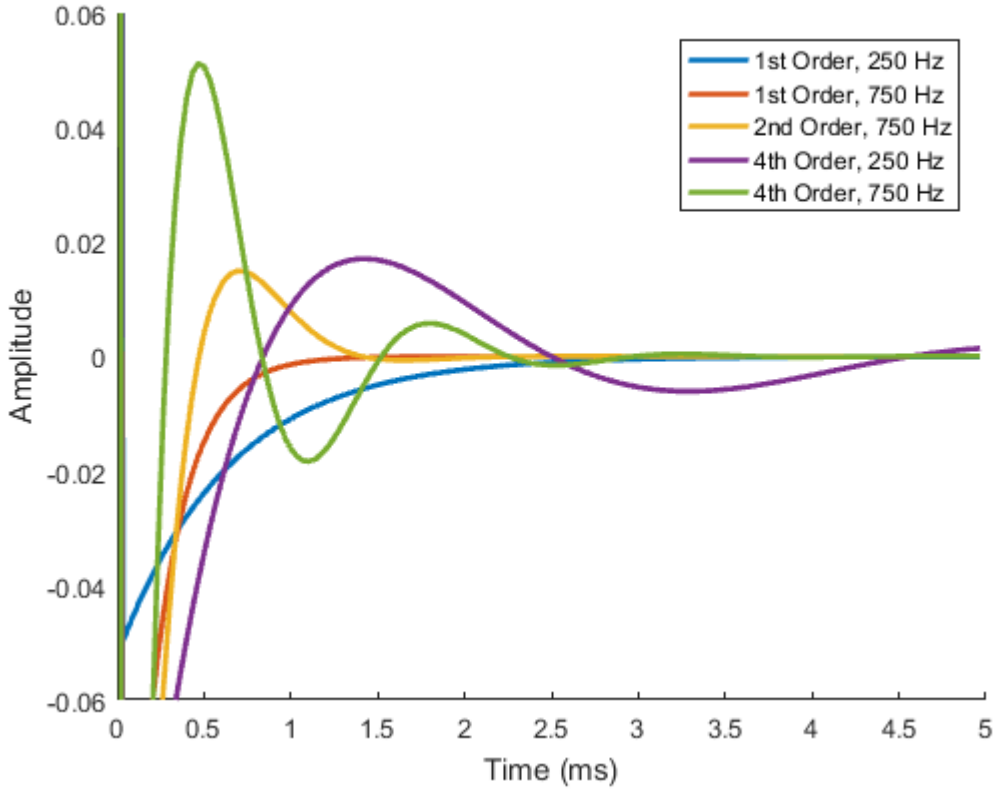

Figure 2.5: High-pass Butterworth impulse responses. Lower order filters oscillate less in response to a perturbation, while higher cutoff frequencies have exhibit faster settling times.

plementation was a first-order Butterworth high-pass filter with a 750 Hz cutoff frequency, which was chosen due to its elimination of filter ringing and fast settling time. These features reduce, but do not eliminate, the distortion of the stimulus artifact. Further increases in cutoff frequency, while resulting in faster settling times, would attenuate much of the signal power in the spike band, commonly cited as approximately 300–6000 Hz [Quian Quiroga, 2009, Stark and Abeles, 2007], with much of the information at about 1000 Hz [Irwin et al., 2016]. While the 750 Hz cutoff frequency is within this band, most of the spike signal is preserved because of the first-order filter's gradual roll-off, as shown in Figure 2.7.

2.3.3 Signal blanking

Stimulation waveforms are distorted by IIR spike filters, resulting in long duration artifacts. The first-order 750 Hz high-pass filter described in Section 2.3.2 reduces, but does not eliminate, this distortion after the end of the stimulus pulse. We implemented a method of blanking the recorded signal during pulse delivery to both reject primary stimulus artifacts and avoid contaminating the filter input with large impulses. Signal blanking was implemented in hardware to ensure that primary stimulus artifacts were eliminated before the digital filtering step. This was achieved using a digital sample-and-hold in the amplifiers. The stimulator was configured to output a TTL synchronization signal beginning 60 microseconds before each stimulation pulse was delivered. This signal was then input to a "blanking circuit," which uses a monostable multivibrator to generate pulses of a fixed duration defined using a potentiometer. The TTL blanking signal output of this circuit, triggered by the rising edge of the stimulator synchronization output, was input to the amplifiers to gate the recording during stimulation by enabling the sample-and-hold feature 60 microseconds before each stimulation pulse, and resuming recording shortly after each stimulation pulse.

While signal blanking is effective at removing primary stimulus artifacts, additional artifacts are caused by discontinuities at the offset of blanking. These discontinuities, while smaller in amplitude than the primary stimulus artifact, often approximate a step input. Just as the impulse-like nature of the primary stimulus artifact produces an approximate

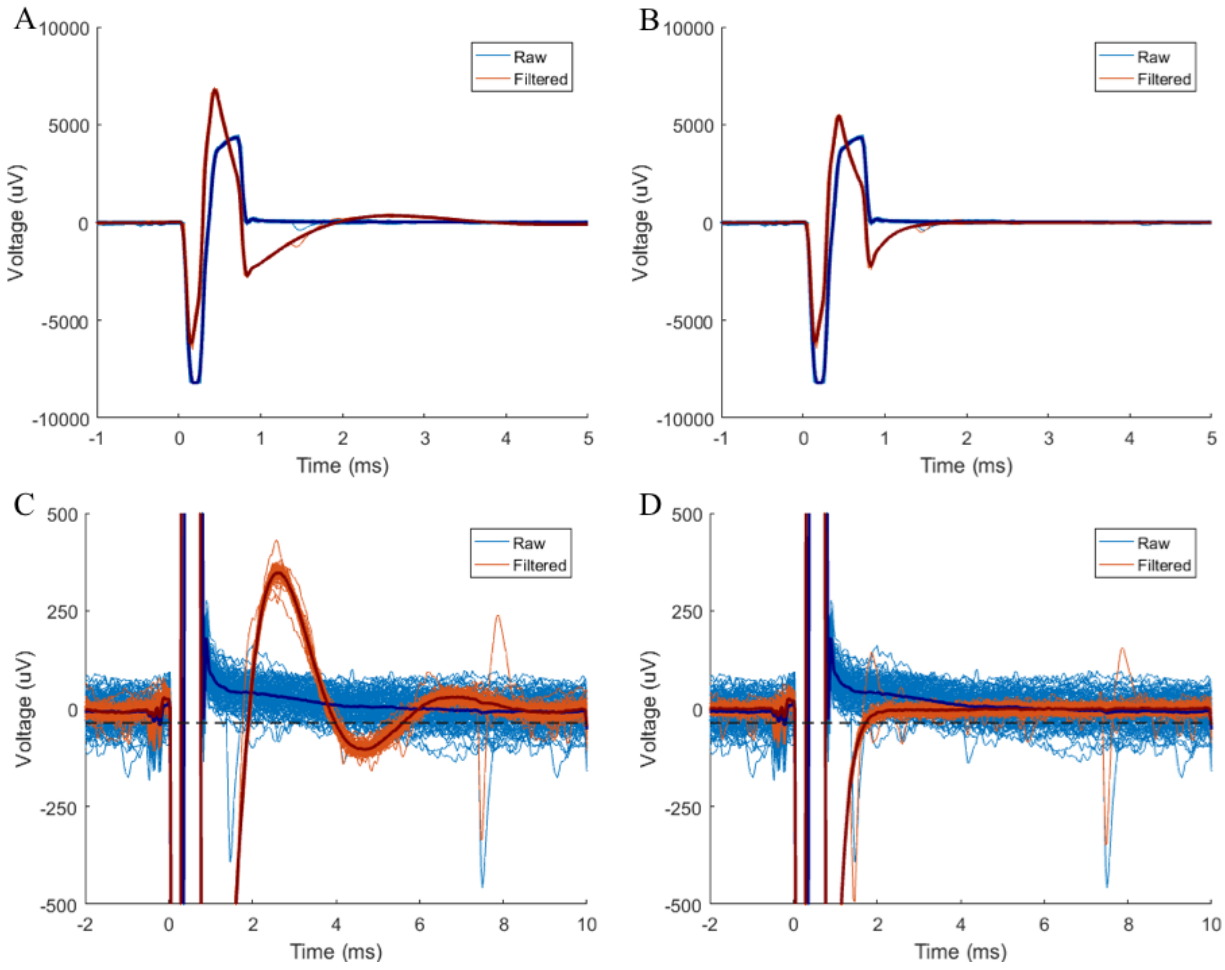

Figure 2.6: Effect of filtering microstimulation artifacts. Each figure shows 100 voltage traces aligned to microstimulation (blue), with a mean trace in dark blue. Filtered signals appear in orange with a mean trace in red. (A) Fourth-order 250 Hz high-pass Butterworth. Distortion and ringing are present in the filtered signal. (B) First-order 750 Hz high-pass Butterworth. Ringing is eliminated but some distortion is still present. (C) and (D) Detailed views of (A) and (B). Dashed gray-lines indicate thresholds used for spike detection.

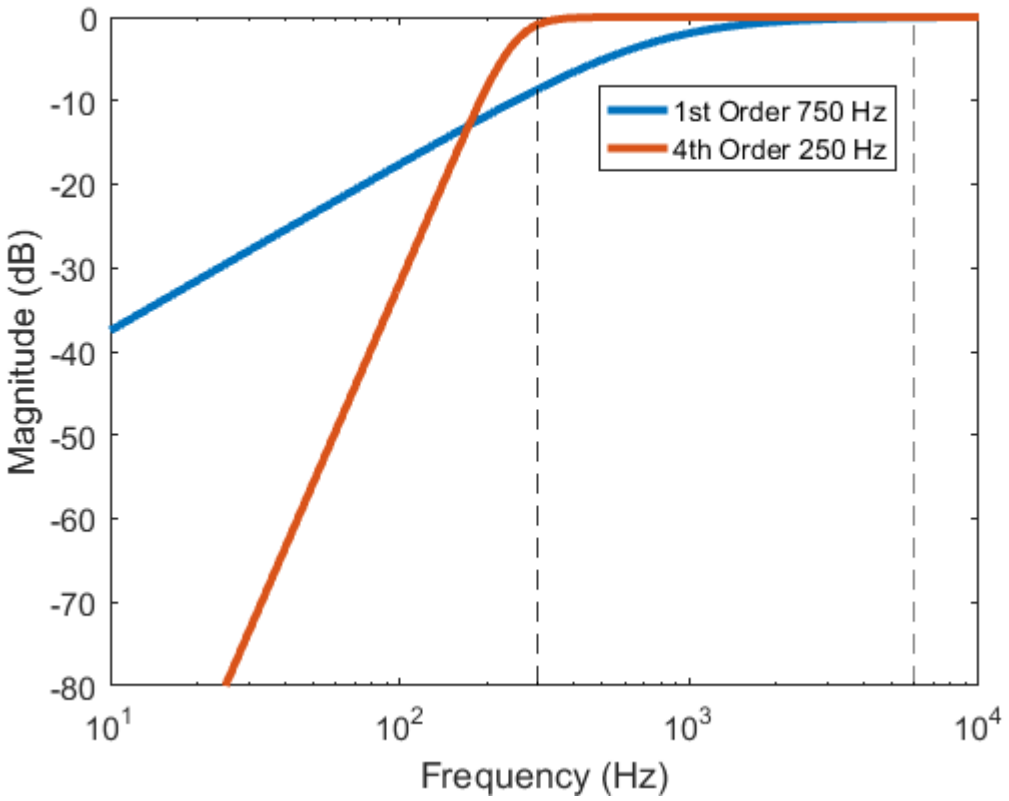

Figure 2.7: Frequency responses of two high-pass Butterworth filters. The edges of the spike power band (300–6000 Hz) are denoted by dashed vertical lines. Despite the first-order filter's higher cutoff frequency, much of the power in the spike band is preserved due to the filter's gradual roll-off.

impulse response, the step-like nature of the blanked signal produces an approximate step response. Therefore, the criteria used to tune the digital filters in Section 2.3.2 still apply after blanking the primary stimulus artifact. The combination of signal blanking and a digital filter with short impulse and step responses can be used to eliminate stimulus artifacts and resume the ability to detect spikes shortly after each stimulus pulse.

The recorded voltage signals were blanked during each stimulation pulse using a sample-and-hold period of 1467 microseconds (44 samples at 30 kHz) triggered by the onset of the synchronization signal output by the stimulator 60 microseconds before each stimulation pulse. This includes 60 microseconds before each stimulation pulse, 700 microseconds while the stimulator is delivering current, and an additional 707 microseconds as the voltage begins to recover from the anodal phase, which in some cases saturates the amplifier. The effect of blanking the signal prior to filtering with either a fourth-order 250 Hz high-pass filter or first-order 750 Hz filter are shown in Figure 2.8. In the final implementation, one additional sample was blanked in software, after the application of the digital filter and threshold, to discard occasional false spikes caused by the discontinuity at the offset of the blanking period. This allows for reliable spike detection as soon as 740 microseconds after the offset of each stimulus pulse and a total signal-blanking duration of 1500 microseconds. The histogram in Figure 2.9, generated from a representative closed-loop stimulation trial, demonstrates that after the blanking period, the distribution of spikes in the inter-stimulus period approximates a uniform distribution.

2.3.4 Signal quality

As discussed in Section 2.3.2, the spike filter was tuned to quickly return to steady state after perturbations related to stimulation. However, the filter parameters also have an effect on overall signal quality. To investigate the effects of high-pass cutoff frequency on signal quality, we performed an analysis based on the band-pass filter analysis in [Lempka et al., 2011] using neural recordings in the absence of ICMS. We validated that increasing the high-pass cutoff frequency resulted in a decrease in peak-to-peak voltage, yet an overall increase in signal-to-noise ratio (SNR). We repeated this analysis using a first-order high-pass filter

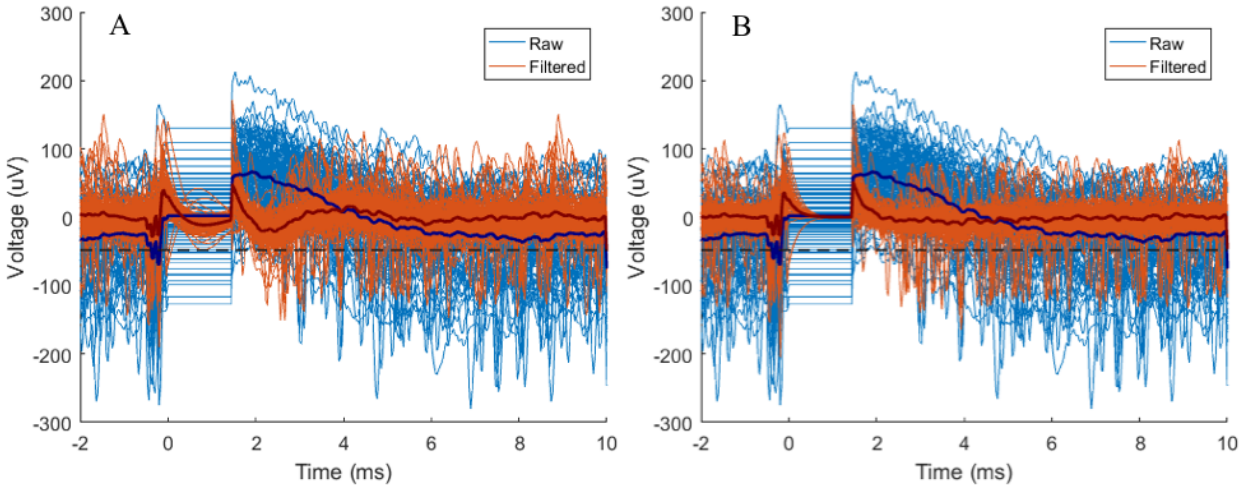

Figure 2.8: Recordings with blanking and filtering during microstimulation. Each figure shows 100 post-blanking voltage traces aligned to microstimulation (blue), with a mean trace in dark blue. Filtered signals appear in orange with a mean trace in red. Dashed gray-lines indicate thresholds used for spike detection. (A) Fourth-order 250 Hz high-pass Butterworth. Some ringing persists in the filtered signal despite the use of blanking. (B) First-order 750 Hz high-pass Butterworth. Signal exhibits a fast settling time without undesired threshold crossings.

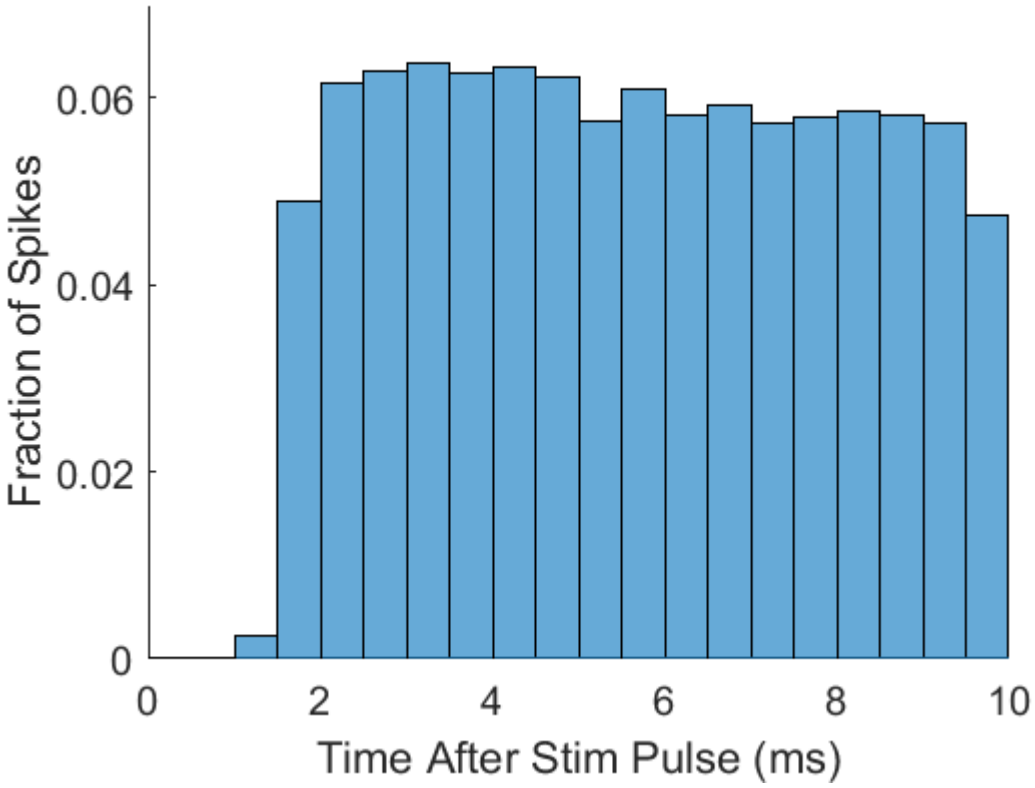

Figure 2.9: Distribution of spikes during inter-stimulus interval. Spikes are absent during the blanking period, but are uniformly distributed during the remainder of the inter-stimulus interval.

and found the same trend to be true. The relationships of cutoff frequency on peak-to-peak voltage, noise level, and SNR are shown in Figure 2.10.

2.3.5 Closed-loop BCI control

The complete artifact rejection scheme was validated online in a closed-loop BCI control task, in which the subject was required to transfer an object across a table as many times as possible in two minutes using a BCI-controlled robot arm. Microstimulation was triggered by the reaction torque measured at the index finger motor as the robot hand contacted the object. Task performance for each condition (no stimulation, stimulation without blanking, and stimulation with blanking for both the fourth-order 250 Hz high-pass filter and first-order 750 Hz high-pass filter) is summarized in Figure 2.11. A one-way analysis of variance revealed a significant difference in number of transfers between task conditions ($F(5, 12) = 75.64, p < 0.001$). Post-hoc Tukey tests revealed no significant differences between the two no stimulation conditions ($p = 0.462$). The number of transfers performed with the artifact rejection scheme with the first-order filter was not significantly different from either the no stimulation fourth-order filter condition ($p = 0.761$) or the no stimulation first-order filter condition ($p = 0.994$). Performance was significantly impaired compared to no stimulation for all other conditions ($p < 0.001$).

2.4 DISCUSSION

We sought to implement a scheme for ICMS artifact rejection that would enable us to develop a closed-loop brain computer interface. We were able to do this by making only minor modifications to an FDA-approved clinical system. By reducing the order of our high-pass Butterworth digital spike filter from fourth-order to first-order, we eliminated oscillatory ringing in the filter output after stimulus pulses. Furthermore, we decreased the settling time of the filter output after stimulation by increasing the cutoff frequency from 250 Hz to 750 Hz. By blanking the signal prior to digital filtering, we were able to reduce the size of

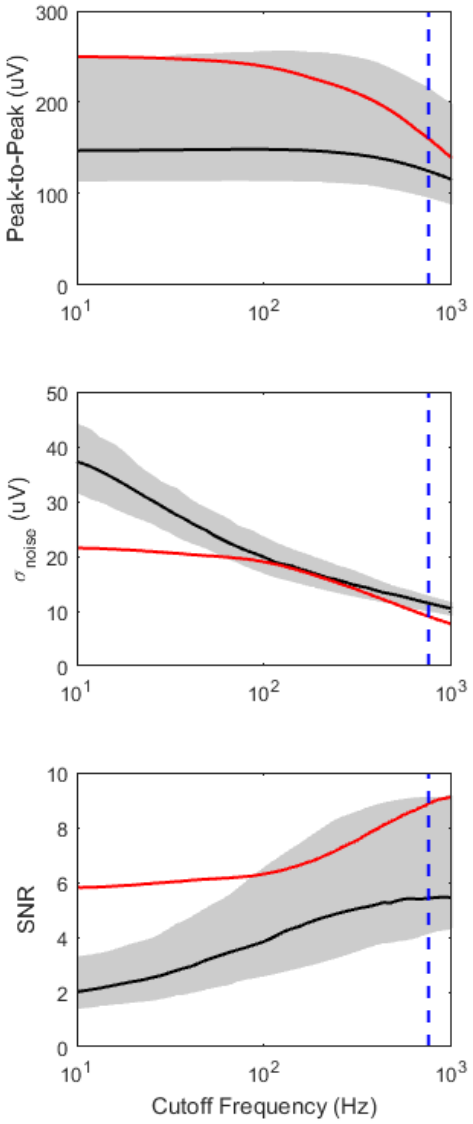

Figure 2.10: Relationship between high-pass cutoff frequency and signal quality. Black lines and gray areas indicate median and interquartile ranges. Red lines are results from [Lempka et al., 2011], included for comparison. Blue dashed lines highlight 750 Hz. (Top) Peak-to-peak voltage decreases with increasing cutoff frequency. (Middle) Noise estimate decreases with increasing cutoff frequency. (Bottom) SNR increases with cutoff frequency.

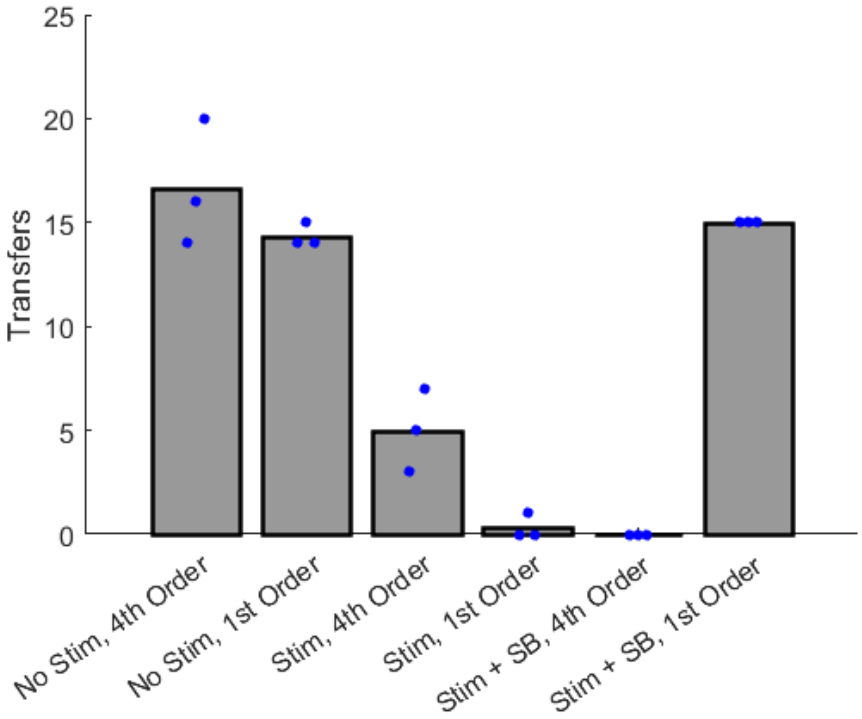

Figure 2.11: Closed-loop BCI task performance. Bars indicate mean number of object transfers per condition. Blue dots indicate number of object transfers for each trial. SB refers to the use of signal blanking, while 4th and 1st order refers to the high-pass filter used.

the perturbation introduced to the filters and further reduce the magnitude of the filter's response to stimulation. Our system allows for spike detection as soon as 740 microseconds after the offset of each stimulus pulse. The increased cutoff frequency also resulted in an overall increase in signal-to-noise. We demonstrated that the introduction of ICMS did not impair functional BCI performance with the artifact rejection scheme in place.

The proposed artifact rejection scheme is simple to implement with standard clinical BCI hardware and has few parameters, allowing it to be easily tuned for different subjects and experiments. Unlike other methods, there is no type of training required. The blanking duration can be varied to favor preserving neural data or eliminating artifact from the raw signal. The high-pass filter cutoff frequency can also be tuned to balance peak-to-peak voltage with fast settling times and high SNR. The scheme also functions with monopolar microstimulation and makes no assumptions about amplifier saturation, unlike proposals that necessitate the use of bipolar stimulation to localize the magnitude and volume affected by artifact [O'Doherty and Sabes, 2016]. Alternative approaches to artifact rejection often rely on complex modeling and signal processing to estimate and subtract templates, or even noncausal algorithms [O'Shea and Shenoy, 2018]. These methods may be useful tools for offline analysis, but may be difficult to adapt to a robust real-time system. When continuous high-bandwidth raw data is collected during stimulation, such as in the development phase of this study, a variety of methods can be applied for offline analysis that would be challenging to implement in real-time due to limitations related to hardware and the need for fast, causal signal processing.

There are several limitations of our proposed scheme. Notably, the use of signal blanking results in a loss of neural data. When stimulating at 100 Hz, a total blanking duration of 1500 μs yields a 15% loss of neural data. In some cases, it may be possible to reduce the signal blanking duration and recover additional spikes. For example, using shorter, symmetric stimulus pulses is likely to be an effective method of reducing the blanking duration. From a practical BCI perspective, we have found that this loss of data has a negligible impact on performance and the method is very effective as long as synchronous stimulus pulses are used with a sufficiently low pulse rate. A model presented by [Young et al., 2018] suggests that decoder SNR is expected to drop off with the square root of the fraction

of blanked data ($\text{SNR}_{\text{Blanked}} = \text{SNR}(\sqrt{1-b}), b =$ fraction of blanked data). This model predicts that our decoder experiences a 7.8% decrease in SNR during 100 Hz stimulation, but this theoretical decline in decoder performance did not manifest as a measurable decrease in task performance.

In the future we may choose to generate biomimetic asynchronous pules on many electrodes. This would lead to cases where stimulation pulses are constantly occurring, and an artifact rejection approach relying on signal-blanking would fail. In this case, another solution such as amplifiers with a higher input range that can fully sample both artifacts and spike signals or different modalities of recording and stimulation, such as optical methods, may be required.

Another limitation is that the parameters must be tuned for worst-case scenarios since the implementation is global and blanks all channels for an equal duration for each stimulation pulse, regardless of artifact amplitude. When stimulation currents are low, the artifacts are less severe and spikes could likely be recovered much closer to the offset of stimulation. A system that automatically adjusts blank time based on stimulation amplitude or electrode location could theoretically perform better, but at the expense of added complexity and less generalizability. A simpler modification that may improve performance would be to linearly interpolate during the blanking period rather than holding a constant value. This computation would require a delay in processing and could not be implemented sample-by-sample in real-time, but would eliminate discontinuities at the offset of blanking. In this case the blanking duration could theoretically be reduced to the duration of the stimulus pulse plus any transients caused by the analog filters. This method cannot be easily implemented with our hardware, but could be implemented by processing the raw digital signals for spike extraction in software. Our method takes advantage of the capabilities of the Neural Signal Processors, but this limited our ability to modify the default signal processing scheme. Processing the raw signals in software would permit much more flexibility to pre-process the signals before applying a digital filter, much like when raw data is processed offline.

Finally, first-order filters have undesirable characteristics in the frequency domain. The filter's frequency response has a wide transition band with gradual roll-off, and thus a large range of frequencies below the cutoff frequency are only partially attenuated. This can be

seen in the filter output during stimulation; low-frequency responses to stimulation are not entirely filtered out and thus the mean filtered signal is not DC during stimulation. While the amplitude of this variation is small, it does bring the mean signal closer to or further from the threshold at various time points, which may affect the sensitivity of detecting low SNR peri-threshold spikes in a time-varying manner. Despite the undesirable frequency domain characteristics of the first-order filter, we chose this filter due to its favorable time-domain characteristics, specifically the absence of ringing in the impulse response. Because the increase in high-pass cutoff frequency resulted in a faster settling time, it is possible that some ringing can be tolerated from a higher order Butterworth filter if the cutoff frequency is increased to yield a sufficiently fast settling time. This would result in a steeper roll-off and better attenuation of low frequencies, but at the expense of attenuating lower frequencies within the spike power band.

Several unanswered questions and future steps may yield further improvements to the system. First, it is unclear what effect the changes in filter order and cutoff frequency have on unit discriminability. While SNR increases with high-pass cutoff frequency, peak-to-peak voltage decreases. This decrease in peak-to-peak voltage may affect the ability to distinguish multiple units. In recent years, spike sorting has fallen out of favor in the BCI community [Chestek et al., 2011, Fraser et al., 2009, Oby et al., 2016, Trautmann et al., 2017], but this may be of concern to groups interested in studying single units. Second, only IIR Butterworth filters[2] were investigated in this study. Finite impulse response (FIR) filters, by definition, can be defined to have a short impulse response and may outperform the first-order IIR filter used here. However, FIR filters typically require many coefficients to perform well in the frequency domain. Finally, modifying the scheme to linearly interpolate during the blanking period, while adding complexity to the system, is likely to yield significant performance gains without introducing more parameters requiring tuning.

[2]Additional discussion of first-order IIR filters is presented in Appendix A.

3.0 REACTION TIMES TO INTRACORTICAL MICROSTIMULATION OF HUMAN SOMATOSENSORY CORTEX

The contents of this chapter are in preparation for submission as a journal article by: Jeffrey M. Weiss, Grace A. Brueggman, Sharlene N. Flesher, Jennifer L. Collinger, and Robert A. Gaunt.

In this chapter, I characterize reaction times to single-channel microstimulation of primary somatosensory cortex for a man with tetraplegia due to a cervical spinal cord injury. The data presented in this chapter provide insight about the rate that we can expect ICMS to transfer information to a BCI user as feedback.

3.1 INTRODUCTION

Brain-computer interfaces (BCIs) have enabled users with tetraplegia to control end effectors such as computer cursors [Hochberg et al., 2006, Pandarinath et al., 2017, Simeral et al., 2011], robotic arms [Collinger et al., 2013, Wodlinger et al., 2014], or even their own hands and arms via functional electrical stimulation [Ajiboye et al., 2017, Bouton et al., 2016]. However, all of these systems lack somatosensory feedback, which able-bodied people depend on for dexterous object manipulation and reaching in the absence of vision. Intracortical microstimulation (ICMS) of somatosensory cortex has been proposed as a method to add sensory feedback to BCI systems [Bensmaia and Miller, 2014, Weber et al., 2012]. We recently demonstrated that ICMS of primary somatosensory cortex can generate graded, focal tactile sensations in a human subject [Flesher et al., 2016], an encouraging result suggesting that ICMS is a viable method to generate naturalistic feedback in a closed-loop BCI. However,

questions remain regarding the information transfer ability of ICMS. For example, a 2014 study found that ICMS cues resulted in much slower responses than visual or vibrotactile cues in a task in a which a monkey was required to redirect to a different target mid-reach after cue presentation [Godlove et al., 2014]. This result was surprising, as one might expect reaction times to ICMS to be faster than natural tactile stimulation, given that ICMS bypasses peripheral conduction with delays typically exceeding 20 ms [Antfolk et al., 2013]. Conflicting results were found in earlier studies. In one experiment, rats were found to perform a discrimination task faster when stimulated with ICMS in auditory cortex versus auditory stimuli [Otto et al., 2005a, Otto et al., 2005b]. Monkeys exhibited indistinguishable reaction times between ICMS of somatosensory cortex and vibrotactile stimuli in a similar discrimation task [Romo et al., 2000]. However, slow reaction times to single-channel ICMS of V1 were noted in, to our knowledge, the only prior attempt to characterize reaction times to ICMS of human cortex [Schmidt et al., 1996].

Previous studies have shown that delayed auditory feedback can impair speech production [Yates, 1963], and delayed visual or auditory feedback can affect motor performance in target tracking tasks [Wargo, 1967], and we suspect that delayed tactile feedback will similarly impair motor performance. We posit that reaction times to ICMS must be similar to those of natural sensory input in order for ICMS to be a viable source of feedback. If ICMS cannot be detected and interpreted with sufficiently low latency, it is unlikely to transmit information quickly enough to be useful for dexterous motor control tasks.

Here, we characterize reaction times to single-channel ICMS of somatosensory cortex in a human with tetraplegia due to spinal cord injury (SCI). We tested the hypothesis that ICMS reaction times would be faster than reaction times to peripheral stimuli by directly comparing ICMS reaction times to electrical stimulation on a region of the participant's hand with spared sensation. We characterized reaction times to ICMS electrodes with projected fields in regions with and without spared sensation to evaluate our hypothesis that the ability to respond to ICMS is unaffected by SCI. We also compared the participant's reaction times to visual and peripheral electrical stimulation with an able-bodied control group to evaluate the generalizability of our results to a larger population.

3.2 METHODS

3.2.1 Participants

A 30-year-old right-handed male (subject CRS2[1]) with a chronic C5 motor/C6 sensory AIS B spinal cord injury enrolled into this study as part of a broader study evaluating the long-term use of a closed-loop BCI. CRS2 was implanted with four Utah microelectrode arrays (Blackrock Microsystems, UT), including two 2.4 mm $\times$ 4 mm arrays of 32 functional sputtered iridium oxide film (SIROF) electrodes in area 1 of left primary somatosensory cortex (S1) and two 4 mm $\times$ 4 mm arrays of 88 functional platinum electrodes in the hand and shoulder areas of left primary motor cortex (M1). The SIROF arrays were used to deliver ICMS from a Cerestim R96 microstimulator (Blackrock Microsystems, UT). CRS2 had been implanted for approximately two years prior to collecting the data presented here. Details of the implantation are described in [Flesher et al., 2016].

Four healthy, right-handed, able-bodied control (ABC) subjects were recruited to compare CRS2's reaction times to a sample normative population. This subject group included two males and two females, with ages ranging from 24–31 (mean 27.5) years old. Each ABC subject was tested in a single test session.

3.2.2 Reaction time paradigm

All subjects were seated in front of a TV screen and provided with either a) a push button (Jelly Bean Twist, AbleNet, MN), or b) a bite switch (Conceptus, AZ) for recording reaction time responses. Subject CRS2 used the bite switch exclusively due to motor deficits resulting from his SCI. Able-bodied subjects were tested with both response methods to evaluate the differences between each method. A green LED was placed in front of each subject to present visual stimuli. Stimulating electrodes were applied to each subject's right arm and hand to provide peripheral electrical stimulation. A ground electrode was placed on each subject's elbow (3M Red Dot, MN), and an adhesive bar electrode (PT30, The Electrode Store, WA) was placed on the lateral side of the PIP joint on the second digit (D2).

[1]Subject CRS2 is the same subject that was described in Chapter 2.

A fixation cross appeared on the TV during each trial to inform the subject that a trial was active, although gaze direction was not systematically controlled. The fixation cross disappeared during a one second inter-trial period between each trial. A longer break was offered after every 20 trials. In each session, a minimum of 5% of trials were catch trials in which no stimulus appeared. In all other trials, one of three possible stimuli occurred after a random delay (0.25–4 s). The three possible stimuli were 1) a visual pulse emitted by a green LED (visual), 2) a 100 Hz train of electrical stimulation pulses applied to D2 (e-stim), or 3) a 100 Hz train of single-channel ICMS pulses (ICMS). Only subject CRS2 received ICMS, as described in Section 3.2.4. All stimuli were 500 ms in duration. E-stim pulses were symmetric anodal-leading biphasic pulses with 200 μs phase widths, delivered using an isolated pulse stimulator (A-M Systems Model 2100, WA). ICMS pulses were asymmetric, charge-balanced pulses with a 200 μs cathodal phase followed by a 100 μs interphase and a 400 μs anodal phase. Stimulus and response times were recorded as digital events with $33\frac{1}{3}$ μs resolution using a Neuroport Neural Signal Processor (Blackrock Microsystems, UT). All stimuli were presented in blocks of at least 60 trials (for subject CRS2) or 100 trials (ABC subjects). Additional trials were collected if multiple trials were failed due to the subject becoming distracted or if the e-stim amplitude needed to be adjusted. ABC subjects repeated the visual stimulus condition with both response methods, the bite switch and the push button. All other conditions were evaluated using only the bite switch. Subject CRS2 repeated a subset of tasks in a total of 12 sessions over a 7 month period, with individual tasks repeated between 3 and 7 times, as detailed in Section 3.2.4.

3.2.3 Detection thresholds and e-stim amplitude

Electrical stimulation (e-stim) detection thresholds were determined by gradually increasing the stimulation amplitude during a continuous 100 Hz pulse train until the subject reported the stimulation was just-noticeable. This procedure was repeated a minimum of three times until a consistent value was determined. For ABC subjects, e-stim amplitudes during the reaction time paradigm were determined by stimulating at 2× threshold, and reducing the amplitude as necessary to a comfortable and salient level. In some cases, this level was

adjusted during breaks due to decreases in perceived intensity after repeated stimulation. Such adjustments were typically on the scale of 0.1–0.2 mA. Thresholds were measured again for ABC subjects at the conclusion of the e-stim block to confirm there were no large changes in threshold during the session.

E-stim thresholds for CRS2 were only measured during three sessions, using the same method as ABC subjects. For subject CRS2, the amplitude was set each day to match the perceived intensity of ICMS channel 19 at 100 μA. This channel features a projected field in the D2 PIP joint of CRS2's hand. The e-stim bar electrode was placed in an attempt to match this projected field. The e-stim amplitude was set by alternating between ICMS and e-stim stimulation, and adjusting the e-stim amplitude until CRS2 could not determine which stimulus was more intense.

Detection thresholds for ICMS channel 19 were measured at the beginning of each session using a two-alternative forced-choice staircase procedure, as described in [Flesher et al., 2016]. Detection thresholds for all other tested ICMS electrodes were recorded in a single session after the conclusion of all other experiments. Data previously published in [Flesher et al., 2016] suggest that, for most ICMS electrodes, detection thresholds do not undergo significant changes over time. As part of a separate series of experiments based on methods described in [Flesher et al., 2016], projected field location and sensation quality were documented for each tested ICMS electrode at 60 μA.

3.2.4 ICMS reaction time subtasks

Subject CRS2 completed three variations of the reaction time paradigm to characterize CRS2's reaction times to a total of four ICMS electrodes. In all variations, reaction times to visual stimuli were collected as a control for day-to-day variability and to compare with ABC data.

In the first variation, repeated in a total of 7 sessions, CRS2's reaction times to channel 19, an electrode on the lateral S1 array, were characterized. This electrode exhibits a projected field in a region of CRS2's hand with spared sensation, and thus the e-stim electrode was placed during each session in an attempt to match the perceived location on the index finger.

Reaction times were collected for channel 19 at 100 μA and for e-stim at an amplitude with approximately equal perceived intensity, as judged by CRS2.

In the second variation, ICMS channel 46, an electrode on the medial S1 array with a projected field in an insensate region of CRS2's hand, was characterized. This variation was repeated in 6 sessions. This channel was compared with previously-characterized channel 19 because CRS2 could not detect e-stim in the same perceived location. Reaction times were collected for channel 46 at 100 μA and for channel 19 at an amplitude with approximately equal perceived intensity, as judged by CRS2.

Finally, reaction times for one additional ICMS electrode on each array were characterized in three sessions to evaluate generalizability across electrodes. Channel 22, on the lateral array, has a projected field similar to channel 19 in a region of the hand with spared sensation. Likewise, channel 54, on the medial array has a projected field in an area of CRS2's hand without intact sensation. Reaction times were collected in response to both of these electrodes at 100 μA.

3.2.5 Reporting of projected fields and sensation qualities

Projected field locations and sensation qualities were documented for each ICMS electrode at 60 μA as part of regular psychophysical surveys. CRS2 drew receptive fields using a Windows 10 tablet (Surface Pro 4, Microsoft, WA) and described the quality of each sensation using a survey previously presented in [Flesher et al., 2016], as well as descriptors of his own choice. A summary of the reported qualities for each tested ICMS electrode was compiled along with representative projected field drawings from several psychophysical surveys conducted within the time course of this study.

3.2.6 Statistical analysis

Due to the expected and observed positive skew of reaction time distributions [Ratcliff, 1993, Whelan, 2008], median and interquartile ranges (IQR) are reported for each reaction time distribution and non-parametric tests (Mann-Whitney U, Brown-Forsythe test for equality of variances) were used to make all statistical comparisons. Bonferroni correction for multiple

comparisons was applied where appropriate, and discrepancies between tests performed with and without correction are noted. The ex-Gaussian distribution, a three-parameter (μ, σ, τ) distribution formulated by the convolution of an exponential and Gaussian distribution and commonly used to model reaction time distributions [Ratcliff, 1993, Whelan, 2008], was fit to reaction time distributions as a visualization aid.

3.3 RESULTS

3.3.1 Comparison of CRS2 with control group

Median and interquartile range (IQR) reaction times to electrical and visual stimulation are listed for each subject and response method in Table 3.1, along with median and IQR reaction times pooled across ABC subjects for each stimulus and response condition. While CRS2 exhibited slower median reaction times than the pooled ABC group for both e-stim and vision (Mann-Whitney U, $p < .001$), his IQR for both e-stim and vision overlapped with the ABC group IQR. CRS2's visual reaction times were significantly different than the visual reaction times of two of the four ABC subjects (Mann-Whitney U, $p < .001$). The outcome of the tests were not affected by Bonferroni correction. After Bonferroni correction, CRS2's e-stim reaction times were significantly different than the e-stim reaction times for three of the four ABC subjects (Mann-Whitney U, $p < .001$). Without Bonferroni-correction, CRS2's e-stim reaction times were significantly different than all four ABC subjects ($p < .05$), though his median reaction times were faster than two of the ABC subjects, and slower than the remaining two ABC subjects' reaction times.

Significant variation was seen across all subjects. All able-bodied subjects had reaction time distributions that were significantly different than all other able-bodied subjects for both e-stim and vision (Mann-Whitney U, $p < .001$). The outcome of the tests were not affected by Bonferroni correction. The differences in reaction time to e-stim across subjects may be due in part to differences in detection thresholds and test amplitudes for each subject. Mean detection threshold and test amplitude values are listed for each subject in Table 3.2.

Table 3.1: Reaction times to electrical and visual stimulation. Reported as median (IQR) in milliseconds.

Subject	E-Stim	Visual	Visual (Button Response)
ABC1	418.8 (369.4–494.7)	302.3 (276.1–345.8)	290.5 (261.9–337.8)
ABC2	224.0 (206.4–257.8)	245.8 (227.6–268.8)	212.7 (198.2–236.6)
ABC3	255.4 (222.9–295.2)	243.7 (228.6–260.2)	201.2 (183–4-216.7)
ABC4	351.4 (324.0–392.3)	322.2 (282.5–358.3)	235.1 (205.5–276.6)
ABC Median	316.5 (246.0–391.2)	270.5 (242.5–316.4)	225.9 (201.3–273.4)
CRS2	339.0 (312.4–369.3)	307.1 (284.0–338.1)	

Detection threshold and test amplitudes for CRS2 were higher than for all ABC subjects, most likely due to sensory deficits related to his spinal cord injury.

Overall, reaction times to visual stimuli were significantly faster than to e-stim, for both the pooled ABC group (Mann-Whitney U, $p < .001$), and CRS2 ($p < .001$). With Bonferroni correction, significant differences between the two modalities were seen in all ABC subjects ($p < .001$), except for ABC3 ($p = .047$). While the full subject population was overall slower to respond to e-stim than visual stimuli, subject ABC2 responded significantly faster to e-stim than to visual stimuli ($p < .001$).

Table 3.2: Detection thresholds and test values for electrical stimulation.

Subject	Mean Threshold (mA)	Mean Test Value (mA)
ABC1	1.2	2.2
ABC2	1.4	2.6
ABC3	1.5	2.8
ABC4	1.1	1.9
CRS2	2.3	3.3

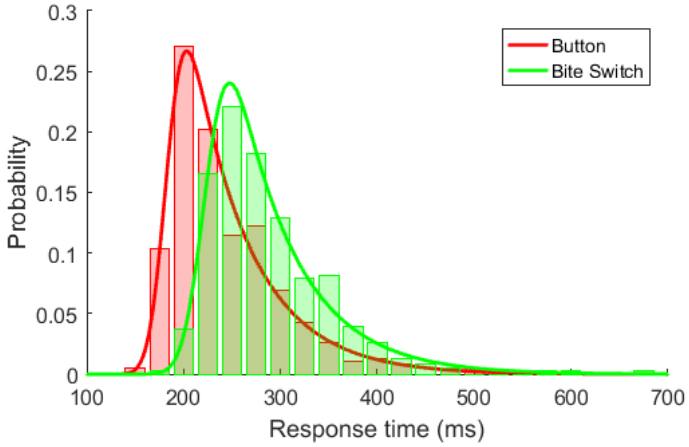

Figure 3.1: Reaction times measured with a bite switch and push button across the ABC group.

The difference between each response method for visual stimulation is also evaluated for each ABC subject and across subjects in Table 3.1. The distributions for each response method pooled across the ABC group is displayed in Figure 3.1. Across the ABC group, median reaction times to visual stimuli were 44.6 ms slower when subjects responded with a bite switch compared to a push button (Mann-Whitney U, $p < .001$). The variance of the reaction time distribution was unaffected by response method (Brown-Forsythe test, $p = .5848$). Within-subjects, visual reaction times using the two response methods were significantly different for three of the four subjects with Bonferroni correction (Mann-Whitney U, $p < .001$). Without correcting for multiple comparisons, the two response methods were significantly different for all four subjects ($p < .05$), and button responses were always faster than bite switch responses.

Trial failures were rare for all participants. No catch trials were failed by any participants. ABC subjects failed to respond to at most 2 trials, and at most 1 trial per condition (approximately 1% of trials per condition). Across sessions, subject CRS2 failed to respond in less than 3% of trials for all conditions, with most of these failures (11/14 failures) occur-

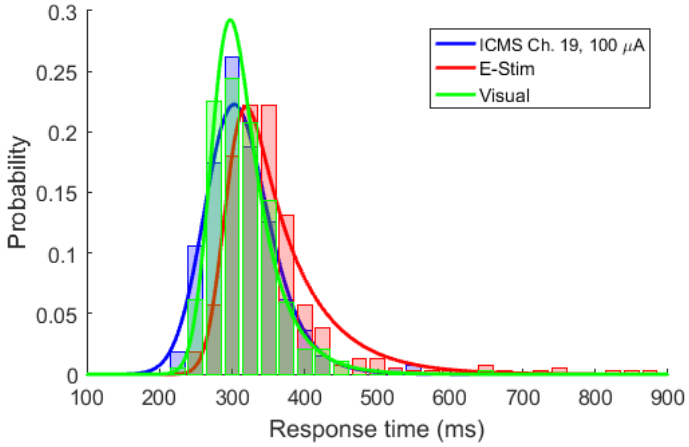

Figure 3.2: Reaction times to single-channel ICMS and e-stim with matched perceived location and intensity. Distributions are pooled across 7 sessions.

ring in the e-stim condition. When necessary, additional trials were collected to compensate for failed trials or if the e-stim amplitude needed to be adjusted.

3.3.2 Reaction times to ICMS and e-stim

Subject CRS2's reaction times to ICMS channel 19, e-stim, and visual stimuli were measured across 7 sessions. Channel 19 was always stimulated at 100 μA, and the e-stim amplitude was set each session to match the perceived intensity of ICMS channel 19. The location of the e-stim electrode was also placed to align with the projected field of ICMS channel 19. The reaction time distributions for ICMS channel 19, e-stim, and visual stimuli pooled across 7 sessions are displayed in Figure 3.2. Across the 7 sessions, the median (IQR) reaction times were 307.0 ms (280.0–338.1) for ICMS, 339.0 ms (312.4–369.3) for e-stim, and 307.1 ms (284.0–338.1) for visual stimuli.

Median ICMS reaction times were significantly faster than median e-stim reaction times when pooled across days (Mann-Whitney U, $p < .001$). After Bonferroni correction, reaction

times to ICMS and e-stim were significantly different in 6 of 7 sessions, 5 of which exhibited faster ICMS reaction times (Mann-Whitney U, $p < .001$). Without Bonferroni correction, ICMS reaction times were also faster than e-stim in the seventh session ($p < .01$). Visual reaction times were also significantly faster than e-stim reaction times when pooled across sessions (Mann-Whitney U, $p < .001$), and in 4 out of 7 sessions ($p < .001$). This result was unaffected by Bonferroni correction. The difference between reaction times to ICMS and visual stimuli was less clear. Pooled across sessions, there was no significant difference (Mann-Whitney U, $p = .3225$). Within sessions and with Bonferroni correction, ICMS was significantly faster than visual stimuli in 2 of 7 sessions ($p < .001$). Without Bonferroni correction, ICMS was significantly faster in 3 sessions ($p < .05$), while vision was significantly faster in 2 sessions ($p < .05$). The remaining 2 sessions had non-significant differences with or without Bonferroni correction. Despite this day-to-day variability, there does not appear to be a real difference between reaction times to this ICMS channel and to visual stimuli.

3.3.3 Reaction times to additional ICMS electrodes

Reaction times to ICMS channel 46 were characterized across 6 sessions. This channel has a projected field in a region of CRS2's hand that is completely insensate as a result of his spinal cord injury, and thus was not directly compared against e-stim. In each of the 6 sessions, reaction times to ICMS channel 46 were compared against visual stimuli and the previously-characterized channel 19 (see Section 3.3.2). Channel 46 was always stimulated at 100 μA, while channel 19 was stimulated at an amplitude with a comparable perceived intensity, which varied across sessions (mean $\pm$ standard deviation amplitude $= 57.7 \pm 9.16$ μA). The reaction time distributions for these two ICMS channels and visual stimuli pooled across sessions are shown in Figure 3.3. Across sessions, the median (IQR) reaction times were 345.7 ms (315.6–382.3) for channel 46, 336.3 ms (307.9–368.0) for channel 19, and 300.3 ms (271.6–332.8) for visual stimuli.

Median reaction times to channel 19 were slightly faster than to channel 46 in 4 of 6 sessions, but when pooled across days this difference was not significant with Bonferroni correction (Mann-Whitney U, $p = .0277 > .0167$). Within days, reaction times to channel

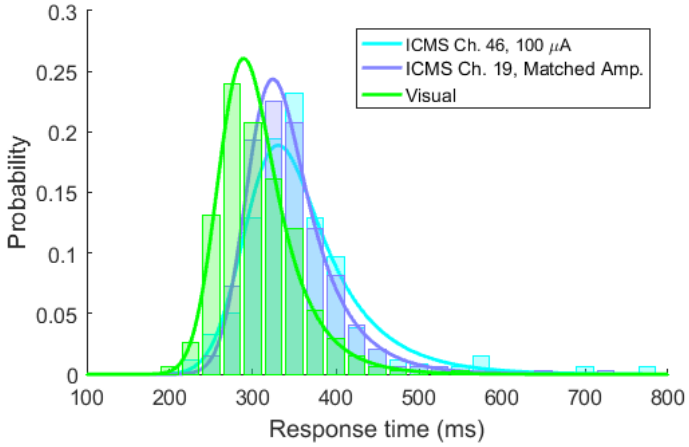

Figure 3.3: Reaction times to ICMS electrodes with a projected fields in sensate (Ch. 19) and insensate (Ch. 46) areas of the hand, at a matched perceived intensity. Distributions are pooled across 6 sessions.

19 were significantly faster than channel 46 for two sessions ($p < .001$), while channel 46 was faster than 19 in a third session ($p < .001$). Reaction times for each channel were not significantly different in the remaining three sessions ($p > .05$). The results of these within-day comparisons were not affected by Bonferroni correction. When pooled across days, median reaction times to visual stimuli were faster than either ICMS electrode (Mann-Whitney U, $p < .001$). Within sessions, this result held up for each electrode for 5 of 6 sessions with Bonferroni correction ($p < .001$), and all 6 sessions without Bonferroni correction ($p < .05$).

Two additional ICMS electrodes, one from each S1 array, were tested in 3 sessions. One electrode, channel 22, had a projected field in a location similar to that of channel 19 (characterized in Section 3.3.2), which is a sensate region of CRS2's hand. The other electrode, channel 54, has a projected field similar to that of channel 46, in an insensate region of CRS2's hand. Both channels were stimulated at 100 μA, without attempting to control for perceived intensity. The reaction time distributions for these two ICMS electrodes

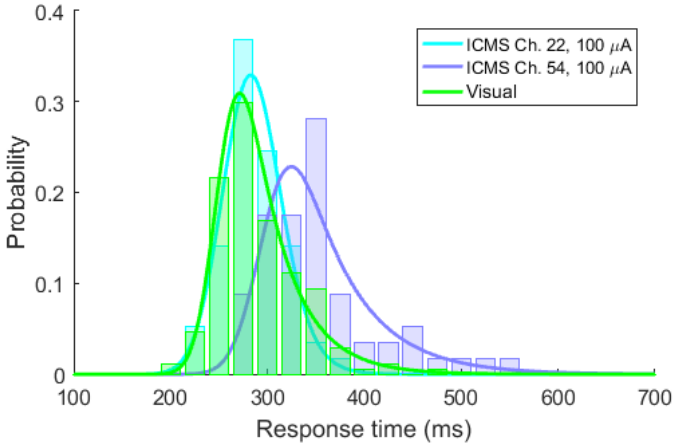

Figure 3.4: Reaction times for two additional ICMS electrodes. Channel 22 has a projected field in a sensate area, while Channel 54 has a projected field in an insensate area. Distributions are pooled across 3 sessions.

and for visual stimuli pooled across 3 sessions are displayed in Figure 3.4. Across sessions, the median (IQR) reaction times were 278.2 ms (259.8–299.9) for channel 22, 341.6 ms (309.2–379.4) for channel 54, and 282.8 ms (260.0–312.7) for visual stimuli.

The median reaction times for ICMS channel 22 were significantly faster than channel 54, both when pooling across sessions (Mann-Whitney U, $p < .001$), and within each session ($p < .001$), without any affect of Bonferroni correction. Reaction times to visual stimuli were also significantly faster than to ICMS channel 54, when pooling across sessions ($p < .001$) or within each session ($p < .001$), without any affect of Bonferroni correction. Pooling across days, there was no significant difference between median reaction times to ICMS channel 22 and visual stimuli ($p = .069$). Within days, reaction times to channel 22 were significantly faster than to visual stimuli in 1 session ($p = .0019 < .01$), with no significant differences in the other two sessions ($p > .05$). There was no effect of Bonferroni correction. A summary of the median (IQR) reaction times to all four tested ICMS electrodes at 100 μA and comparisons to other channels and modalities is presented in Table 3.3.

Table 3.3: Summary of median reaction times to four ICMS electrodes at 100 μA and comparisons to other modalities. * denotes that channel 19 was stimulated at an amplitude to match the perceived intensity of channel 22.

Channel	Median (IQR) Reaction Time (ms)	Relation to other modalities
19	307.0 (280.0–338.1)	19 $\approx$ visual $<$ e-stim
22	278.2 (259.8–299.9)	22 $\approx$ visual
46	345.7 (315.6–382.3)	visual $<$ 46 $\approx$ 19*
54	341.6 (309.2–379.4)	visual $<$ 54

3.3.4 Properties of tested ICMS electrodes

The detection thresholds for each tested ICMS electrode, measured at the end of the study, are listed in Table 3.4. Detection thresholds for ICMS channel 19 were recorded before every session, as part of an on-going long-term ICMS stability study. For the 12 sessions presented here, the mean $\pm$ standard deviation detection threshold for channel 19 was 11.2 ± 2.8 μA. The additional three electrodes were only tested in the final 6 sessions, which spanned a shorter time period. In these 6 sessions, the mean $\pm$ standard deviation detection threshold for channel 19 was 12.4 ± 1.6 μA. The stability of channel 19's threshold across days, combined with the detection threshold stability data presented in [Flesher et al., 2016], suggest that thresholds on the other channels were likely stable throughout the course of the study.

The projected field locations for each tested ICMS electrode at 60 μA, as drawn by CRS2 in a separate experiment, are shown in Figure 3.5, and a summary of the sensations elicited by each electrode at this amplitude are summarized in Table 3.4. It is worth noting that CRS2 described channel 22 as the most focal of the four electrodes tested. This electrode also had the lowest detection threshold, but was not described as the most intense of the four electrodes at 100 μA. The relative intensities of each electrode were not systematically studied, but based on discussions with CRS2, each electrode at 100 μA can most likely be ranked from most to least intense in the following order: 19, 46, 22, 54.

Table 3.4: ICMS detection thresholds and sensation qualities.

Channel	Array	Threshold (μA)	Sensation Quality Summary
19	Lateral	12.4	Sharp pressure and buzzy vibration
22	Lateral	6.4	Pressure, tingle, and some vibration
46	Medial	8.8	Slightly sharp pressure and warm tingle
54	Medial	17.4	Pressure and tingle

3.4 DISCUSSION

In this study, we characterized simple reaction times to single-channel ICMS of primary somatosensory cortex in a human participant, and compared against reaction times to visual stimuli and electrical stimulation in the periphery for the same subject and able-bodied controls. Overall, we found significant overlap between reaction time distributions for ICMS, e-stim, and visual stimuli (see Figure 3.2). For most subjects, responses to visual stimuli were significantly faster than to e-stim. Reaction times to ICMS varied across channels (see Table 3.3), but reaction times to two of four ICMS channels were not significantly different than to visual stimuli, and, for the only channel in which a direct comparison was made, reaction times to ICMS were significantly faster than to e-stim by approximately 32 ms, a result one might expect given conduction delays of 20 ms or more from the periphery [Antfolk et al., 2013] (see Section 3.3.2).

Reaction times to two other ICMS electrodes were significantly slower than to vision by approximately 63–74 ms. One of these two electrodes was compared directly against channel 19, which was previously characterized as eliciting reaction times significantly faster than to e-stim, and not significantly different than to visual stimuli, by reducing the amplitude on channel 19 to control for perceived intensity. Reaction times to these two electrodes were not significantly different. Assuming similar relationships between perceived intensity and reaction time for ICMS and peripheral e-stim, it is possible that other electrodes would also elicit faster reaction times than to e-stim when controlling for perceived intensity.

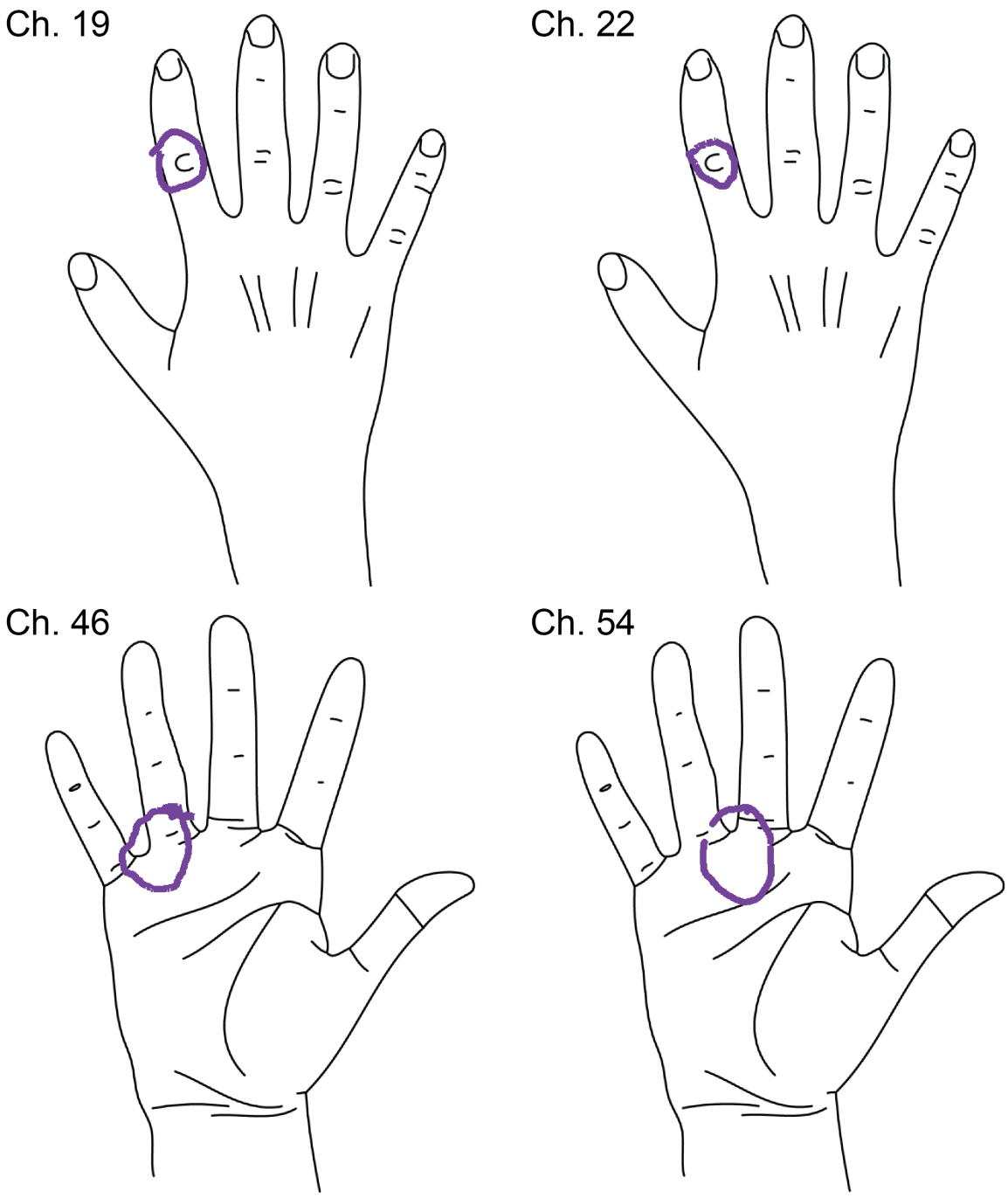

Figure 3.5: Projected fields for tested ICMS electrodes, as drawn by CRS2.

We observed considerable variability across subjects (see Table 3.1), sessions, and ICMS electrodes (see Table 3.3). Comparing e-stim and ICMS reaction times across subjects, sessions, and electrodes is inherently difficult due to the known relationship between reaction time and stimulus intensity [Kohfeld, 1971, Teichner, 1954, Teichner and Krebs, 1972], a parameter which is difficult to control for, particularly with tactile and electrical stimuli. Using multiples of detection threshold has limitations [Zele et al., 2007], as does self-reported perceived intensity. In an attempt to minimize the effect of perceived intensity on reaction time, we attempted to only use stimuli that were sufficiently suprathreshold such that small changes in intensity would have minimal effect on reaction time [Kohfeld, 1971, Teichner and Krebs, 1972]. Furthermore, we attempted to match the intensities of ICMS and e-stim (see Section 3.3.2) and of two ICMS channels (see Section 3.3.3) for direct comparison.

Several prior studies evaluated reaction times to ICMS in various areas of cortex. Schmidt et al. evaluated reaction times to phosphenes generated by ICMS of primary visual cortex in a blind human participant [Schmidt et al., 1996]. Like our study, Schmidt only tested ICMS in a single participant, and only tested a small number of microelectrodes. Based on previous studies of reaction times to surface stimulation of visual cortex, Schmidt expected reaction times as fast as 175 ms, but found that reaction times to ICMS were slower than expected (means of 395 and 452 ms for two electrodes). Schmidt did not directly compare ICMS reaction times against other stimulus modalities or subjects, but noted the decrease in reaction time with increasing stimulation amplitude in prior studies, as well as the known relationships between reaction time and brightness and size of a visual stimulus. In Schmidt's study, electrodes were always stimulated at 1.5× threshold during reaction time trials. Based on their presented threshold data, this suggests amplitudes of approximately 20 μA were used in reaction time trials, considerably less than the 100 μA amplitude used in our study, although they used a longer pulse-width (600 μs).

Several animal studies provided choice reaction time data during discrimination tasks involving ICMS. Romo found that reaction times to ICMS of area 3b of S1 were indistinguishable compared to vibrotactile stimuli in a flutter frequency discrimination task [Romo et al., 2000]. Mean reaction times to vibrotactile (324 ms) and ICMS (339 ms) were not significantly different. Stimulation amplitudes varied between 65 μA and 100 μA. Otto et al.

used ICMS of auditory cortex in rats during an auditory frequency discrimination task [Otto et al., 2005a, Otto et al., 2005b]. The authors found that ICMS of auditory cortex at 68 μA evoked significantly faster choice reaction times than auditory stimuli by more than 290 ms. The authors interpreted their results as suggesting that the ICMS stimuli were more salient than the auditory stimuli but made no other claims about the differences in reaction times to each modality, acknowledging that the results were dependent on the stimulus parameters and behavioral task.

Our results suggest that, for at least one electrode and when controlling for intensity, reaction times to ICMS of area 1 of S1 are faster than to e-stim by approximately 32 ms. However, conflicting results were presented in an earlier study by Godlove et al. [Godlove et al., 2014]. In Godlove's study, a monkey responded slower to ICMS cues than to visual or vibrotactile cues in a redirect reaching task by approximately 70 ms (vibrotactile) and 50 ms (visual). These differences were decreased in a simpler pressured reaction time task, in which ICMS reaction times were approximately 50 ms slower than vibrotactile cues, and 15 ms slower than visual cues. Additionally, two monkeys and a cohort of human subjects responded faster to vibrotactile stimuli than to visual stimuli. In our study, most subjects responded more slowly to electrical stimulation than to visual stimulation. It is possible that electrical stimulation recruited a different population of afferents than vibrotactile stimulation, but electrical stimulation is generally believed to recruit the largest diameter axons first [McNeal, 1976], which have the fastest conduction velocities [Goldman and Albus, 1968]. There are mixed results in the literature comparing the reaction times to visual and tactile stimuli (e.g. [Diederich and Colonius, 2004, Forster et al., 2002]), suggesting that comparing these modalities is sensitive to specific task conditions. It is likely that discrepancies are related to differences in perceived intensity of the stimuli in each experiment. Stimulus intensity is a well-known correlate of reaction time [Kohfeld, 1971, Teichner, 1954, Teichner and Krebs, 1972], and can be difficult to control across experiments, subjects, sessions, and even within sessions due to issues such as consistent placement of the electrode or transducer, changes at the electrode-skin interface, or habituation. Additionally, the fact that the monkey in Godlove's study required significant training to perform the task with ICMS raises doubts about the saliency of the ICMS cue in the monkey.

It is also worth noting the difference in response methods between studies. The methods used to capture reaction times is known to significant effects, both in terms of the body part used to respond [Teichner, 1954], as well as the apparatus and criteria used to determine the time of response [Smeets and Brenner, 2017]. In our study, participants responded using a bite switch, and able-bodied controls also responded to visual stimuli with a push button for comparison. While we determined that reaction times were slower when responding with a bite switch than a push button, we assumed that any differences between response methods were independent of stimulus modality. In [Godlove et al., 2014], response time was measured as the difference between stimulus time and reach reversal (zero-velocity) time in a reaching task. It is possible that this response method, which was more complex and involved larger movements than our study, impacted their results.

In [Godlove et al., 2014], stimulus types were interleaved, and during the redirect reach task, redirect stimuli only appeared in 30% of trials. Reaction times are known to be slower when stimuli are interleaved [Boulter, 1977], which is why we chose to use a block design. Boulter found that visual reaction times were more affected by interleaved modalities than tactile reaction times [Boulter, 1977], suggesting that visual reaction times may have been disproportionately slowed in Godlove's study due to the interleaved task design. Finally, differences in anatomy may explain discrepancies between the two studies. We found that the ICMS electrode with the most focal projected field elicited the fastest reaction times (see Section 3.3.4, Table 3.3). While more data is required to determine if a causal relationship exists between ICMS projected field size and reaction time, it is nonetheless worth mentioning that it is unclear if such focal projected fields can be expected in a monkey due to the differences in anatomical scale between species, resulting in compressed somatotopic organization in monkeys. A study by Gregg Tabot et al. found that monkeys trained to perform a location discrimination task with mechanical indentations could continue performing the task when one or both mechanical stimuli were replaced with ICMS trains, but the monkeys' performance suggested that ICMS projected fields were more diffuse than mechanical indentations [Tabot et al., 2013].

We hypothesized that reaction times to ICMS would be faster than to peripheral electrical stimulation because ICMS bypasses peripheral circuits and associated conduction delays.

However, it can be argued that this hypothesis is overly simplistic, as it is unclear if there are differences in cortical processing of ICMS and peripheral sensory input to generate a response. ICMS indiscriminately and synchronously recruits neurons near the electrode tip, leading to unnatural patterns of activity [Tabot et al., 2015]. It is possible that such unnatural activity needs additional processing before it can drive downstream circuits to generate a response. Godlove suggested that the need for signal amplification and refinement could explain the slow ICMS responses observed in his study [Godlove et al., 2014]. Because stimulation in S1 bypasses the brainstem and thalamus, additional sensory areas that would normally be recruited in parallel with S1 are either not recruited at all or are activated in an unnatural way after S1 drives output to other areas. It is also possible that ICMS may have different effects on independent streams of cortical processing for conscious perception and reaction, unconscious reflexes (e.g. long-loop reflexes to prevent object slip [Picard and Smith, 1992]), updating of feedforward models, and motor learning.

While additional data is required to resolve the discrepancies between various studies of ICMS reaction times, we find our result encouraging. CRS2's reaction times were generally slower than the ABC group, which may have been related to his spinal cord injury, or may have been an artifact of insufficient sample size, as considerable variation was seen across subjects. Alternatively, factors related to sleep quality, medication usage, or other health factors may explain the observed significant differences in reaction times. Regardless, we find the intra-subject comparisons between modalities compelling. If reaction times to ICMS are similar to, and perhaps even faster than, reaction times to peripheral e-stim or visual stimuli, we suspect that ICMS can provide information quickly enough to be a useful source of feedback for BCI users. Future studies should evaluate reaction times to ICMS at different amplitudes, reaction times to multi-channel stimulation, and the ability to quickly interpret ICMS in more meaningful ways, such as discriminating between force levels as encoded by ICMS amplitude or frequency. A choice reaction time paradigm may be an effective method to evaluate the ability to quickly discriminate between different ICMS parameters.

4.0 SUMMARY AND CONCLUSIONS

In the years before starting this work, significant advances had been made in the field of intracortical brain-computer interface (BCI), starting with rodent research in the late 1990s [Chapin et al., 1999], to nonhuman primate work [Taylor et al., 2002], and the first demonstration of a human with tetraplegia using an intracortical BCI to control a cursor in 2006 [Hochberg et al., 2006]. In the following decade, progressively better BCI control was achieved, allowing for as many as ten simultaneously controlled degrees-of-freedom of a robotic arm [Wodlinger et al., 2014]. However, all of these demonstrations required the BCI user's visual attention at all times, as no alternative forms of feedback were provided. Able-bodied people depend on somatosensory feedback to perform dexterous tasks and control their limbs in the absence of vision. The loss of either tactile or proprioceptive sensation results in substantial deficits to motor control [Gordon et al., 1995, Johansson and Flanagan, 2009, Monzee et al., 2003, Rothwell et al., 1982]. The need to include some form of nonvisual sensory feedback in a BCI system had been recognized, and intracortical microstimulation (ICMS) had been proposed as a solution (e.g. [Abbott, 2006, Weber et al., 2012]).

Shortly before starting the work presented here, our lab demonstrated for the first time that ICMS of somatosensory cortex could evoke naturalistic tactile percepts that are focal and graded with amplitude in an individual with tetraplegia [Flesher et al., 2016], an encouraging result suggesting that ICMS has the potential to restore sensory feedback for BCI users. While several nonhuman primate studies investigated the use of ICMS to provide cues or feedback during BCI control [O'Doherty et al., 2009, O'Doherty et al., 2011], questions remained about whether or not ICMS was a viable method of feedback.

I identified two knowledge gaps that needed to be resolved to demonstrate the viability of ICMS as a method of adding feedback to a closed-loop BCI system. First, questions remained

about the compatibility of ICMS with current intracortical BCI technology. Intracortical BCI uses microelectrodes to record small extracellular potentials from the brain, which are decoded to control end-effectors. ICMS requires large voltages to inject current through high-impedance microelectrodes and produce voltage gradients in the brain that generate action potentials in nearby neurons. This produces large artifacts in the recordings, such as those seen in Figure 2.4. These artifacts mask neural spikes and can saturate the recording amplifiers. Furthermore, applying a high-pass or band-pass filter, which is necessary to extract spike signals for BCI decoding, can distort the artifact, resulting in artifacts that are longer than each stimulus pulse width, and possibly corrupting the recording during the entirety of a stimulus train. While numerous methods for artifact rejection had been proposed, such as interleaved recording and stimulation intervals [O'Doherty et al., 2011], or template subtraction [Limnuson et al., 2014], we required a robust method that would be compatible with our existing FDA-cleared BCI system and allow for uninterrupted recording during continuous ICMS trains.

Second, while we had demonstrated that ICMS could evoke sensations that felt natural [Flesher et al., 2016], questions remained about whether the stimulation could actually be perceived at a rate appropriate for continuous real-time feedback. A 2014 study found, unexpectedly, that a monkey responded more slowly to ICMS cues than to visual or vibrotactile cues [Godlove et al., 2014]. While conflicting results were found in earlier animal studies [Otto et al., 2005a, Otto et al., 2005b, Romo et al., 2000], relatively slow reaction times were also documented in the only known prior attempt to characterize reaction times to ICMS in a human subject [Schmidt et al., 1996]. Such results were troubling, because if a BCI user could not quickly detect and react to microstimulation, the modality would not be suitable for use as a source of continuous real-time feedback to improve motor control in situations requiring rapid responses to perturbations or errors. For example, if an object begins to slip out of one's hand, immediate feedback is needed to generate a motor response to counteract the slipping before the object is dropped. I sought to address this issue by directly testing reaction times to ICMS of somatosensory cortex in a human participant.

In Chapter 2, I presented a method to reject artifacts that was simple, robust, and compatible with our existing BCI system. This method consisted of applying a sample-and-

hold to blank most of the artifact from the recorded signal prior to digital filtering, and updating our digital filter to a first-order 750 Hz high-pass Butterworth filter, which features short impulse and step responses[1] without oscillations. These features allowed spikes to be reliably recorded as soon as 750 μs after the offset of each stimulus pulse. Furthermore, I "closed the loop" of our BCI system by updating the system to record sensor data from a robot and transform the sensor data to stimulation commands. I then validated the artifact rejection method by demonstrating that while the addition of ICMS normally resulted in impaired BCI performance due to stimulus artifacts, my artifact rejection method restored BCI performance to baseline levels.

In Chapter 3, I characterized simple reaction times to single-channel ICMS of somatosensory cortex in a human with tetraplegia due to spinal cord injury. Four electrodes were characterized, including electrodes with projected fields in sensate and insensate regions of the subject's hand. I found that, while the subject's reaction times were generally slower than a small population of able-bodied subjects, his reaction times to ICMS were similar to those for both visual stimuli and electrical stimulation of his hand in a region with intact sensation. For at least one electrode that was directly compared to electrical stimulation, reaction times to ICMS were significantly faster than to peripheral electrical stimulation, a result that was hypothesized based on the fact that ICMS bypasses peripheral afferent pathways with conduction delays exceeding 20 ms [Antfolk et al., 2013], but contradicted results previously reported in a nonhuman primate study [Godlove et al., 2014].

The results presented in Chapters 2 and 3 suggest that ICMS can provide sensory feedback in a closed-loop BCI system that can be quickly perceived by the BCI user and without significant impairments to the neural recordings used for decoding. While additional work is needed, these results demonstrate the feasibility of bidirectional BCI systems that both directly extract information from and transmit feedback to the brain, and the results imply that such systems may allow for more skillful control than current technology allows.

[1] By definition, an infinite impulse response (IIR) filter has an infinitely-long impulse response. The descriptions of "short" or "long" duration impulse and step responses in this thesis refer not to the total length of the response, but to the approximate duration before the filter approaches its steady state value, $\lim_{t\to\infty} h(t)$.

4.1 FUTURE WORK

4.1.1 Artifact rejection

While the work presented in Chapter 2 met the objective of rejecting artifacts while preserving enough neural data to maintain BCI performance, there is still room for improvement in the area of artifact rejection. First, it is unclear that the filter chosen in Chapter 2 is the optimal filter to preserve high-SNR neural data while reducing blank duration. Alternative filter designs, such as finite impulse response (FIR) filters may be capable of outperforming the first-order Butterworth filter. Additionally, the use of a first-order filter may not have been necessary. Increasing the cutoff frequency reduced the duration of the impulse response and led to an increase in SNR ratio. Using a first-order filter eliminated oscillations in the filter response, but at the expense of decreased performance in the frequency domain. If the impulse response is sufficiently short, some oscillation in the impulse response may be tolerable when used in combination with software blanking. However, it is unclear if a filter with a steeper roll-off is actually preferable in this case, as the increase in cutoff frequency causes low frequency components of spike waveforms to be attenuated. In the current scheme, the increase in cutoff frequency is somewhat offset by the gradual roll-off of the first-order filter.

It is also unclear if signal blanking is a crucial component of the artifact rejection scheme. While signal blanking prevents the stimulus waveform from generating a large impulse response in the filter output, it also delays the inevitable step response until the offset of blanking. If an impulse response occurred immediately at stimulus onset and was rejected via software blanking, it is possible that the filter could be tuned to recover more quickly than the current scheme with signal blanking.

Numerous methods such as variations of template subtraction (e.g. [Limnuson et al., 2014, O'Shea and Shenoy, 2018, Wagenaar and Potter, 2002]), or linear regression referencing [Young et al., 2018], have been proposed which aim to recover neural data during the actual stimulus pulse. While we opted for a simpler approach that did not require training data or more complicated signal processing, an ideal solution would not involve any signal blanking and allow spikes to be recorded even during stimulus pulses. However, monopolar ICMS often

results in amplifier saturation, which can both extend the length of the artifact and prevent any possibility of recovering spikes during the stimulus using techniques such as template subtraction. While some researchers have opted to use bipolar stimulation for this reason (e.g. [O'Doherty and Sabes, 2016]), a better solution would be to develop amplifiers with a wider input range such that they can fully sample both stimulus artifacts and coincident spike waveforms without saturating.

4.1.2 ICMS reaction times and encoding of feedback

The work in Chapter 3 demonstrated that reaction times to ICMS of human somatosensory cortex were comparable or slightly faster than reaction times to electrical stimulation in the periphery. However, additional work in needed to address several limitations of this study. First, a relatively small data set was collected for four microelectrodes in a single participant. Additional electrodes and subjects should be tested to evaluate generalizability and to resolve discrepancies between the results of our study and prior studies such as [Godlove et al., 2014]. Second, with one exception (see Section 3.3.3) each electrode was only characterized at its maximum amplitude of 100 μA. Additional amplitudes need to be characterized to confirm that lower amplitudes evoke a sensation that is salient enough to produce adequate reaction times. Finally, the reaction time task is abstract and shares little in common with a functional task in which feedback would be beneficial. Additional work is required to demonstrate that ICMS feedback can be continuously interpreted in a meaningful way to modify behavior during a motor control task. For example, the critical stability task [Quick et al., 2014] is a challenging task which requires an informative feedback signal that can be quickly interpreted to produce rapid corrections in motor output. This task may be appropriate to test how quickly a modulated ICMS signal can be interpreted in the context of a motor control task. Alternatively, a choice reaction time task in which various ICMS parameters must be quickly discriminated is a simple way to extend the reaction time task to require more than stimulus detection.

While the results of [Flesher et al., 2016] and Chapter 3 suggest that ICMS can both evoke naturalistic sensations and be perceived quickly enough to be used for feedback, ques-

tions still remain about how to best encode feedback that can be easily interpreted by the user. As briefly mentioned in Section 1.2, several types of mechanoreceptors exist in the skin, which lead to complex patterns of activity in cortex. In the normal somatosensory system, slowly-adapting and rapidly-adapting afferents encode both dynamic and static components of tactile sensation. Artificial somatosensory feedback such as ICMS should also provide both dynamic and static components of touch. Various methods could be used to encode such information, such as relying on rates of change to indirectly encode dynamic information, linearly superimposing both components onto a signal, or encoding both signals separately using independent electrodes. Alternatively, biomimetic pulse trains based on patterns of spike timing observed in recordings of somatosensory cortex may produce naturalistic sensations containing both dynamic and static information.

4.2 ALTERNATIVES TO ICMS-BASED CLOSED-LOOP BCI

While the work presented in this thesis suggests that ICMS is a promising method to restore useful and naturalistic feedback to BCI users, there are alternative options that may be capable of providing adequate feedback, and even options that may not require the user to receive feedback at all. For example, optogenetics is an alternative method to directly activate neurons in the brain, and has been proposed as an alternative to ICMS for closed-loop BCI [Gilja et al., 2011]. Optogenetics involves using genetic engineering techniques to transfer genes for light-sensitive ion channel proteins to neurons which can then be optically stimulated. This has several advantages, such as the possibility of targeting populations of neurons with more precision than is possible with ICMS, and avoiding artifacts in electrical recordings. While much more research is needed before the use of optogenetics can be attempted in humans, several recent studies have shown that the approach can work in nonhuman primates [Gerits and Vanduffel, 2013].

Additional methods for sensory restoration include non-invasive approaches to provide sensory feedback. For example, rather than attempting to evoke sensations referred to the hand, a sensory substitution approach could take advantage of regions of intact sensation. An

experiment by Paul Bach-y-Rita demonstrated that a person with peripheral sensory deficits could learn to interpret electrical stimuli applied to their forehead as if the sensations were on their hand [Bach-y Rita, 1973, Bach-y Rita and W. Kercel, 2003]. Similar methods have been utilized in attempts to restore sensation to amputees via electrical stimulation of the skin on their residual limb or peripheral nerve stimulation using implanted electrodes [Antfolk et al., 2013].

Alternative solutions may allow for improved control of BCI end effectors without the user receiving any form of sensory feedback. For example, our lab previously demonstrated that BCI control of a robotic limb could be improved by using a shared control approach that blends BCI and autonomous robotics [Downey et al., 2016]. This system attempted to determine the user's intent based on the decoded velocity signal, but allowed the robotic system to handle low-level tasks such as stabilization and achieving the proper orientation to grasp a particular type of object. This concept could be expanded to also apply the correct amount of force on an object, without actually providing force feedback to the user. Richard Andersen has attempted to decode high-level intent signals directly by recording from the posterior parietal cortex [Aflalo et al., 2015], a sensory integration area believed to be involved in motor planning, rather than low-level motor commands that are generated in primary motor cortex [Andersen and Buneo, 2002]. If high-level intent can be reliably decoded, such commands may not depend on constant visual feedback and could be executed by autonomous robotic systems without requiring the user to receive sensory feedback. A downside to such approaches are that by not providing sensory feedback and abstracting low-level control to autonomous systems, it becomes less likely that the user will form a sense of embodiment of the system [Marasco et al., 2011, Tabot et al., 2015]. Thus, it is likely that the ideal solution will involve a combination of assistance from autonomous control systems to improve fine motor control, with naturalistic sensory feedback to enhance a sense of embodiment and inform the user of the state of the system.

APPENDIX A

NOTES ON IIR FILTER TYPES AND FIRST-ORDER FILTERS

The purpose of this appendix chapter is to document some additional details about the selection of a digital filter to reduce the effect of stimulus artifacts. The final outcome of this analysis is presented in Chapter 2.

As discussed in Chapter 2, prior to adding ICMS to our BCI system, we processed our neural data with a 250 Hz high-pass fourth-order Butterworth filter, which is a standard filter implemented in the Blackrock Microsystems Neuroport system. We quickly identified the problem of filter ringing in response to stimulus artifact (see Figure 2.6), and investigated methods to reduce this ringing. Initially, we questioned the choice of a Butterworth filter, and investigated alternative types of infinite impulse response (IIR) filters. We considered the use of Type I Chebyshev filters, which permit ripple in the passband but allow for a steeper roll-off with a lower filter order. Of course, this was a misunderstanding of the cause of the filter ringing, which was not directly related to frequency domain characteristics such as roll-off, but was rather a manifestation of the filter's time domain properties, and in particular the filter's impulse response.

Without a proper understanding of the nature of our problem, we happened to stumble onto an adequate solution. Knowing that the use of a Chebyshev filter would allow us to preserve frequency selectivity while reducing the filter order, we tested various lower order filters and found that a first-order Type I Chebyshev filter completely eliminated the ringing after each ICMS pulse. We also found, somewhat unexpectedly, that this filter design resulted in an increase in signal-to-noise ratio (SNR) despite a decrease in peak-to-peak voltage.

Later, I discovered that similar observations about SNR and peak-to-peak had been made regarding the effect of high-pass cutoff frequency on spike recordings [Lempka et al., 2011].

At this point, I began to dig into the details to better understand the nature of our problem and solution. First, I reviewed the equations for magnitude frequency responses for nth-order Butterworth (Equation A.1) and Type I Chebyshev filters (Equation A.2) with unity DC-gain. Equations for low-pass filters are shown for simplicity, but these observations generalize to high-pass filters. ω denotes frequency, ω_c is the filter's cutoff frequency, ϵ is the ripple factor, and T_n is a nth-order Chebyshev polynomial.

$$|H(j\omega)|^2 = \frac{1}{1 + \left(\frac{\omega}{\omega_c}\right)^{2n}} \tag{A.1}$$

$$|H(j\omega)|^2 = \frac{1}{1 + \epsilon^2 T_n^2\left(\frac{\omega}{\omega_c}\right)} \tag{A.2}$$

Next, I compared the first-order implementations of each filter design. The first-order Chebyshev polynomial is simply $T_1(x) = x$. Therefore, the magnitude frequency responses for first-order low-pass Butterworth (Equation A.3) and Type I Chebyshev filters (Equation A.4) are:

$$|H(j\omega)|^2 = \frac{1}{1 + \left(\frac{\omega}{\omega_c}\right)^{2}} = \frac{1}{1 + \frac{\omega^2}{\omega_c^2}} \tag{A.3}$$

$$|H(j\omega)|^2 = \frac{1}{1 + \epsilon^2\left(\frac{\omega}{\omega_c}\right)^{2}} = \frac{1}{1 + \epsilon^2\frac{\omega^2}{\omega_c^2}} \tag{A.4}$$

The only difference between these two equations is the ϵ parameter in the Type 1 Chebyshev filter equation. Equation A.4 can be rewritten as:

$$|H(j\omega)|^2 = \frac{1}{1 + \frac{\omega^2}{\left(\frac{\omega_c}{\epsilon}\right)^2}} \tag{A.5}$$

After examining this lumped parameter, ω_c/ϵ, what perhaps should have been obvious is now immediately clear: a first-order filter can only have one unique parameter. By designing a first-order Type I Chebyshev filter with cutoff frequency ω_c and ripple factor ϵ, we were really changing the true cutoff frequency, $\omega_{c,true} = \omega_c/\epsilon$.

Thus, all first-order IIR filters are equivalent, and should be specified in simplest terms, i.e. as a single-parameter Butterworth filter. Additionally, the observed increase in SNR can be explained by the fact that by introducing a ripple factor, we were really increasing the cutoff frequency, leading to an increase in SNR as predicted by [Lempka et al., 2011].

APPENDIX B

BCI SOFTWARE DOCUMENTATION

The purpose of this appendix chapter is to provide a brief overview of the closed-loop BCI software system used in Chapter 2. An overview of the hardware and major algorithms (decoding and sensor stimulus transform) was provided in Section 2.2, but the software system was not presented in detail in Chapter 2.

A system diagram of the closed-loop BCI software suite is shown in Figure B1. Neural and digital data including spike snippets are sent over a UDP protocol from two Neural Signal Processors (Blackrock Microsystems, UT) to two instances of SPM_Cerebus, which bin spike snippets into spike counts in 10 ms bins and pass data to SPM_Combiner as `RAW_SPIKECOUNT` messages over the Real-Time Messaging Architecture (RTMA) protocol.[1] SPM_Combiner receives spike count data from one or more instances of SPM_Cerebus and combines the data into 20 ms bins of 256-channel spike counts. This data is output every 20 ms as an `SPM_SPIKECOUNT` message (blue arrows), which is both used for decoding and as a 50 Hz time source for multiple modules throughout the system.

`SPM_SPIKECOUNT` messages are buffered and filtered by the SpikeExtraction module to predict intended velocity commands from estimated firing rates using an optimal linear estimator (OLE) decoder (described in Section 2.2.5.1). In some cases, some degrees of freedom are partially or fully automated by the ActiveAssist module. `CONTROL_SPACE_COMMAND` velocity commands (green arrows) from SpikeExtraction and ActiveAssist are summed by the

[1] RTMA was developed in Andrew Schwartz's lab by Meel Velliste and Sagi Perel. An open-source version named Dragonfly Messaging is hosted at https://github.com/dragonfly-msg/dragonfly.

MPL_Control module, which forms a final velocity command (`FINISHED_COMMAND`), sent over a UDP protocol (MUD) to VulcanX (Applied Physics Laboratory (APL), MD), an interface to control the Modular Prosthetic Limb (MPL) (APL).

MPL sensor data is returned from VulcanX using a UDP protocol and received by the MPL_Feedback module, which forwards limb state data (`CONTROL_SPACE_FEEDBACK`, orange lines) and force and torque data (`MPL_REBIASED_SENSOR_DATA`) to downstream modules using RTMA. `CONTROL_SPACE_FEEDBACK` is received by ActiveAssist to generate automated proportional velocity commands based on current limb state and target positions. `MPL_REBIASED_SENSOR_DATA` is received by the Sensor_Stimulus_Transform module to generate stimulation commands using a linear transformation, as documented in Section 2.2.5.2. At the start of each trial, up to 15 stimulus parameter sets (amplitude, frequency, and pulse-width) are output by Sensor_Stimulus_Transform as `CERESTIM_CONFIG_MODULE` messages. Desired stimulation commands are output as `CERESTIM_CONFIG_CHAN_PRESAFETY` messages, which are checked for safety in the Stim_Safety_Module, and then output as final `CERESTIM_CONFIG_CHAN` messages. `CERESTIM_CONFIG_MODULE` and `CERESTIM_CONFIG_CHAN` messages are received by the Cerestim_Module, which uses the CereStim C++ API to command the Cerestim R96 microstimulator (Blackrock Microsystems).

The Executive module controls the state of the system and experiment flow. Executive outputs `TASK_STATE_CONFIG` messages (gray lines), which contain parameters such as targets, gains, and weights to determine whether each control dimension is controlled by SpikeExtraction, ActiveAssist, or both. Executive determines when Sensor_Stimulus_Transform can output stimulation commands via `TASK_STATE_CONFIG`. Executive also receives limb state `CONTROL_SPACE_FEEDBACK` messages to compare against target positions and evaluate task success.

The Stim_Safety_Module ensures that the following safe stimulation criteria are met:

- Stimulation amplitudes are in the range 0–100 μA
- Stimulation frequencies are in the range 0–300 Hz
- No more than 12 electrodes can be simultaneously stimulated
- The maximum global charge in 144 nC/phase.
- No electrode can be stimulated for more than 1500 pulses/30 s

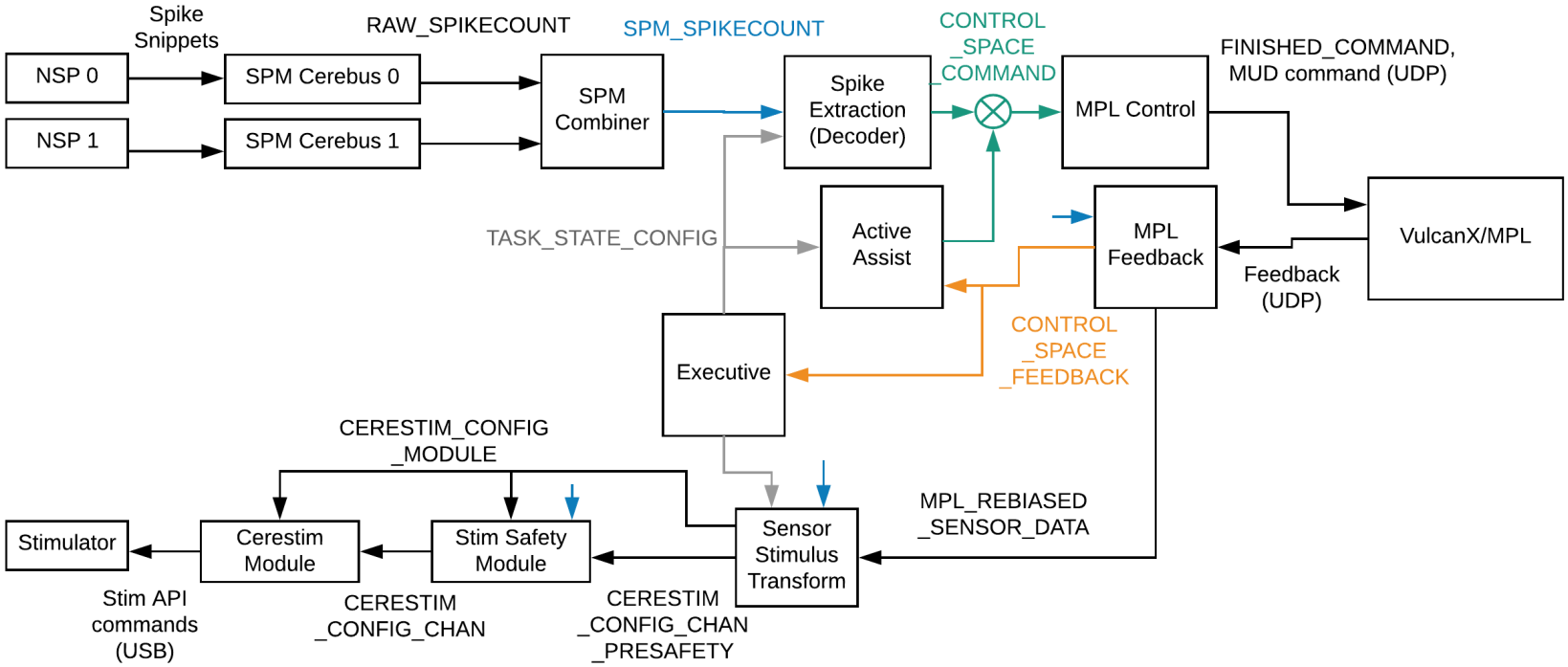

Figure B1: BCI system diagram.

BIBLIOGRAPHY

[Abbott, 2006] Abbott, A. (2006). Neuroprosthetics: In search of the sixth sense. *Nature*, 442(7099):125–127.

[Abraira and Ginty, 2013] Abraira, V. E. and Ginty, D. D. (2013). The sensory neurons of touch. *Neuron*, 79(4):618–639.

[Aflalo et al., 2015] Aflalo, T., Kellis, S., Klaes, C., Lee, B., Shi, Y., Pejsa, K., Shanfield, K., Hayes-Jackson, S., Aisen, M., Heck, C., Liu, C., and Andersen, R. (2015). Decoding motor imagery from the posterior parietal cortex of a tetraplegic human. *Science*, 348(6237):906–910.

[Ajiboye et al., 2017] Ajiboye, A. B., Willett, F. R., Young, D. R., Memberg, W. D., Murphy, B. A., Miller, J. P., Walter, B. L., Sweet, J. A., Hoyen, H. A., Keith, M. W., Peckham, P. H., Simeral, J. D., Donoghue, J. P., Hochberg, L. R., and Kirsch, R. F. (2017). Restoration of reaching and grasping movements through brain-controlled muscle stimulation in a person with tetraplegia: A proof-of-concept demonstration. *The Lancet*, 389(10081):1821–1830.

[Alles, 1970] Alles, D. S. (1970). Information transmission by phantom sensations. *IEEE transactions on man-machine systems*, 11(1):85–91.

[Anani et al., 1977] Anani, A. B., Ikeda, K., and Körner, L. M. (1977). Human ability to discriminate various parameters in afferent electrical nerve stimulation with particular reference to prostheses sensory feedback. *Medical and Biological Engineering and Computing*, 15(4):363–373.

[Andersen and Buneo, 2002] Andersen, R. A. and Buneo, C. A. (2002). Intentional Maps in Posterior Parietal Cortex. *Annual Review of Neuroscience*, 25(1):189–220.

[Antfolk et al., 2013] Antfolk, C., D'Alonzo, M., Rosén, B., Lundborg, G., Sebelius, F., and Cipriani, C. (2013). Sensory feedback in upper limb prosthetics. *Expert Review of Medical Devices*, 10(1):45–54.

[Asanuma, 1981] Asanuma, H. (1981). Microstimulation technique. In *Electrical Stimulation Research Techniques*, pages 61–70. Academic Press New York.

[Asanuma and Sakata, 1967] Asanuma, H. and Sakata, H. (1967). Functional organization of a cortical efferent system examined with focal depth stimulation in cats. *J. Neurophysiol.*, 30:35–54.

[Atkins et al., 1996] Atkins, D. J., Heard, D. C., and Donovan, W. H. (1996). Epidemiologic overview of individuals with upper-limb loss and their reported research priorities. *JPO: Journal of Prosthetics and Orthotics*, 8(1):2–11.

[Bach-y Rita, 1973] Bach-y Rita, P. (1973). Sensory substitution: Neural mechanisms underlying prosthetic applications. *Neural organization and its relevance to prosthetics. New York: Intercontinental Medical Book Corporation*, pages 149–164.

[Bach-y Rita and W. Kercel, 2003] Bach-y Rita, P. and W. Kercel, S. (2003). Sensory substitution and the human–machine interface. *Trends in Cognitive Sciences*, 7(12):541–546.

[Bak et al., 1990] Bak, M., Girvin, J. P., Hambrecht, F. T., Kufta, C. V., Loeb, G. E., and Schmidt, E. M. (1990). Communication: Visual sensations produced by intracortical microstimulation of the human occipital cortex. *Medical and Biological Engineering and Computing*, 28(3):257–259.

[Bartlett and Doty, 1980] Bartlett, J. R. and Doty, R. W. (1980). An exploration of the ability of macaques to detect microstimulation of striate cortex. *Acta Neurobiol. Exp.*, 40(4):713–727.

[Beeker et al., 1967] Beeker, T. W., During, J., and Den Hertog, A. (1967). Artificial touch in a hand-prosthesis. *Medical and biological engineering*, 5(1):47–49.

[Bensmaia and Miller, 2014] Bensmaia, S. J. and Miller, L. E. (2014). Restoring sensorimotor function through intracortical interfaces: Progress and looming challenges. *Nature reviews. Neuroscience*, 15(5):313–25.

[Biddiss and Chau, 2007] Biddiss, E. A. and Chau, T. T. (2007). Upper limb prosthesis use and abandonment: A survey of the last 25 years. *Prosthetics and Orthotics International*, 31(3):236–257.

[Boulter, 1977] Boulter, L. R. (1977). Attention and reaction times to signals of uncertain modality. *Journal of Experimental Psychology: Human Perception and Performance*, 3(3):379–388.

[Bouton et al., 2016] Bouton, C. E., Shaikhouni, A., Nicholas, V., Bockbrader, M. A., Friedenberg, D. A., Nielson, D. M., Sharma, G., Sederberg, P. B., Glenn, B. C., Mysiw, J., Morgan, A. G., Deogaonkar, M., and Rezai, A. R. (2016). Restoring cortical control of functional movement in a human with quadriplegia. *Nature*, 533(7602):247–250.

[Brindley and Lewin, 1968] Brindley, B. Y. G. S. and Lewin, W. S. (1968). The Sensations Produced By Electrical Simulation of the Visual Cortex. *Journal of Physiology*, 196(2):479–493.

[Carmena et al., 2003] Carmena, J. M., Lebedev, M. A., Crist, R. E., O'Doherty, J. E., Santucci, D. M., Dimitrov, D. F., Patil, P. G., Henriquez, C. S., and Nicolelis, M. A. L. (2003). Learning to control a brain-machine interface for reaching and grasping by primates. *PLoS Biology*, 1(2):193–208.

[Carruthers and Pottinger, 1968] Carruthers, M. T. and Pottinger, J. M. (1968). Paper 17: Research into the Possibility of a Substitute for Proprioception. *Proceedings of the Institution of Mechanical Engineers, Conference Proceedings*, 183(10):98–102.

[Chapin et al., 1999] Chapin, J. K., Moxon, K. A., Markowitz, R. S., and Nicolelis, M. A. (1999). Real-time control of a robot arm using simultaneously recorded neurons in the motor cortex. *Nature neuroscience*, 2(7):664.

[Chestek et al., 2011] Chestek, C. A., Gilja, V., Nuyujukian, P., Foster, J. D., Fan, J. M., Kaufman, M. T., Churchland, M. M., Rivera-Alvidrez, Z., Cunningham, J. P., Ryu, S. I., and Shenoy, K. V. (2011). Long-term stability of neural prosthetic control signals from silicon cortical arrays in rhesus macaque motor cortex. *Journal of Neural Engineering*, 8(4).

[Clippinger, 1973] Clippinger, F. W. (1973). A system to provide sensation from an upper extremity amputation prosthesis. *Neural organization and its relevance to prosthetics. London: International Medical Book Corporation.*

[Collinger et al., 2013] Collinger, J. L., Wodlinger, B., Downey, J. E., Wang, W., Tyler-Kabara, E. C., Weber, D. J., McMorland, A. J. C., Velliste, M., Boninger, M. L., and Schwartz, A. B. (2013). High-performance neuroprosthetic control by an individual with tetraplegia. *Lancet*, 381(9866):557–64.

[Cushing, 1909] Cushing, H. (1909). A note upon the faradic stimulation of the postcentral gyrus in conscious patients. *Brain*, 32(1):44–53.

[Dadarlat et al., 2014] Dadarlat, M. C., O'Doherty, J. E., and Sabes, P. N. (2014). A learning-based approach to artificial sensory feedback leads to optimal integration. *Nature Neuroscience*, 18(1):138–144.

[D'Anna et al., 2017] D'Anna, E., Petrini, F. M., Artoni, F., Popovic, I., Simanić, I., Raspopovic, S., and Micera, S. (2017). A somatotopic bidirectional hand prosthesis with transcutaneous electrical nerve stimulation based sensory feedback. *Scientific Reports*, 7(1).

[D'Anna et al., 2018] D'Anna, E., Valle, G., Mazzoni, A., Strauss, I., Ibertie, F., Patton, J., Petrini, F., Raspopovic, S., Granata, G., and Di Iorio, R. (2018). A closed-loop hand prosthesis with simultaneous intraneural tactile and position feedback. *bioRxiv*, page 262741.

[Davis et al., 2016] Davis, T. S., Wark, H. A. C., Hutchinson, D. T., Warren, D. J., O'Neill, K., Scheinblum, T., Clark, G. A., Normann, R. A., and Greger, B. (2016). Restoring

motor control and sensory feedback in people with upper extremity amputations using arrays of 96 microelectrodes implanted in the median and ulnar nerves. *Journal of Neural Engineering*, 13(3):036001.

[Dhillon and Horch, 2005] Dhillon, G. and Horch, K. (2005). Direct Neural Sensory Feedback and Control of a Prosthetic Arm. *IEEE Transactions on Neural Systems and Rehabilitation Engineering*, 13(4):468–472.

[Diederich and Colonius, 2004] Diederich, A. and Colonius, H. (2004). Bimodal and trimodal multisensory enhancement: Effects of stimulus onset and intensity on reaction time. *Perception & psychophysics*, 66(8):1388–1404.

[Dobelle et al., 1974] Dobelle, W. H., Mladejovsky, M. G., and Girvin, J. P. (1974). Artificial vision for the blind: Electrical stimulation of visual cortex offers hope for a functional prosthesis. *Science*, 183(4123):440–444.

[Doty, 1965] Doty, R. W. (1965). Conditioned reflexes elicited by electrical stimulation of the brain in macaques. *Journal of neurophysiology*, 28(4):623–640.

[Doty and Bartlett, 1981] Doty, R. W. and Bartlett, J. R. (1981). Stimulation of the brain via metallic electrodes. In *Electrical Stimulation Research Techniques*, pages 71–103. Elsevier.

[Downey et al., 2017] Downey, J. E., Brane, L., Gaunt, R. A., Tyler-Kabara, E. C., Boninger, M. L., and Collinger, J. L. (2017). Motor cortical activity changes during neuroprosthetic-controlled object interaction. *Scientific Reports*, 7(1):16947–16947.

[Downey et al., 2016] Downey, J. E., Weiss, J. M., Muelling, K., Venkatraman, A., Valois, J.-S., Hebert, M., Bagnell, J. A., Schwartz, A. B., and Collinger, J. L. (2016). Blending of brain-machine interface and vision-guided autonomous robotics improves neuroprosthetic arm performance during grasping. *Journal of neuroengineering and rehabilitation*, 13(1):28–28.

[Eshraghi et al., 2012] Eshraghi, A. A., Nazarian, R., Telischi, F. F., Rajguru, S. M., Truy, E., and Gupta, C. (2012). The Cochlear Implant: Historical Aspects and Future Prospects. *The Anatomical Record: Advances in Integrative Anatomy and Evolutionary Biology*, 295(11):1967–1980.

[Fetz, 1969] Fetz, E. E. (1969). Operant conditioning of cortical unit activity. *Science*, 163(3870):955–958.

[Fitzsimmons et al., 2007] Fitzsimmons, N. A., Drake, W., Hanson, T. L., Lebedev, M. A., and Nicolelis, M. A. L. (2007). Primate Reaching Cued by Multichannel Spatiotemporal Cortical Microstimulation. *Journal of Neuroscience*, 27(21):5593–5602.

[Flesher et al., 2016] Flesher, S. N., Collinger, J. L., Foldes, S. T., Weiss, J. M., Downey, J. E., Tyler-Kabara, E. C., Bensmaia, S. J., Schwartz, A. B., Boninger, M. L., and Gaunt,

R. A. (2016). Intracortical microstimulation of human somatosensory cortex. *Science Translational Medicine*, 8(361):361ra141–361ra141.

[Forget and Lamarre, 1987] Forget, R. and Lamarre, Y. (1987). Rapid elbow flexion in the absence of proprioceptive and cutaneous feedback. *Human neurobiology*, 6(1):27–37.

[Forster et al., 2002] Forster, B., Cavina-Pratesi, C., Aglioti, S. M., and Berlucchi, G. (2002). Redundant target effect and intersensory facilitation from visual-tactile interactions in simple reaction time. *Experimental Brain Research*, 143(4):480–487.

[Fraser et al., 2009] Fraser, G. W., Chase, S. M., Whitford, A., and Schwartz, A. B. (2009). Control of a brain-computer interface without spike sorting. *Journal of Neural Engineering*, 6(5).

[Freeman, 1971] Freeman, J. A. (1971). An electronic stimulus artifact suppressor. *Electroencephalography and clinical neurophysiology*, 31(2):170–172.

[Georgopoulos et al., 1982] Georgopoulos, A. P., Kalaska, J. F., Caminiti, R., and Massey, J. T. (1982). On the relations between the direction of two-dimensional arm movements and cell discharge in primate motor cortex. *Journal of Neuroscience*, 2(11):1527–1537.

[Georgopoulos et al., 1986] Georgopoulos, A. P., Schwartz, A. B., and Kettner, R. E. (1986). Neuronal Population Coding of Movement Direction. *Science*, 233(4771):1416–1419.

[Gerits and Vanduffel, 2013] Gerits, A. and Vanduffel, W. (2013). Optogenetics in primates: A shining future? *Trends in Genetics*, 29(7):403–411.

[Gilja et al., 2011] Gilja, V., Chestek, C. A., Diester, I., Henderson, J. M., Deisseroth, K., and Shenoy, K. V. (2011). Challenges and Opportunities for Next-Generation Intracortically Based Neural Prostheses. *IEEE Transactions on Biomedical Engineering*, 58(7):1891–1899.

[Godlove et al., 2014] Godlove, J. M., Whaite, E. O., and Batista, A. P. (2014). Comparing temporal aspects of visual, tactile, and microstimulation feedback for motor control. *Journal of neural engineering*, 11(4):046025–046025.

[Goldman and Albus, 1968] Goldman, L. and Albus, J. S. (1968). Computation of impulse conduction in myelinated fibers; theoretical basis of the velocity-diameter relation. *Biophysical journal*, 8(5):596–607.

[Gordon et al., 1995] Gordon, J., Ghilardi, M. F., and Ghez, C. (1995). Impairments of reaching movements in patients without proprioception. I. Spatial errors. *Journal of neurophysiology*, 73(1):347–360.

[Grumet, 1999] Grumet, A. E. (1999). *Electric Stimulation Parameters for an Epi-Retinal Prosthesis*. PhD thesis, Massachusetts Institute of Technology.

[Histed et al., 2009] Histed, M. H., Bonin, V., and Reid, R. C. (2009). Direct Activation of Sparse, Distributed Populations of Cortical Neurons by Electrical Microstimulation. *Neuron*, 63(4):508–522.

[Histed et al., 2013] Histed, M. H., Ni, A. M., and Maunsell, J. H. R. (2013). Insights into cortical mechanisms of behavior from microstimulation experiments. *Progress in Neurobiology*, 103:115–130.

[Hochberg et al., 2012] Hochberg, L. R., Bacher, D., Jarosiewicz, B., Masse, N. Y., Simeral, J. D., Vogel, J., Haddadin, S., Liu, J., Cash, S. S., van der Smagt, P., and Donoghue, J. P. (2012). Reach and grasp by people with tetraplegia using a neurally controlled robotic arm. *Nature*, 485(7398):372–5.

[Hochberg et al., 2006] Hochberg, L. R., Serruya, M. D., Friehs, G. M., a Mukand, J., Saleh, M., Caplan, A. H., Branner, A., Chen, D., Penn, R. D., and Donoghue, J. P. (2006). Neuronal ensemble control of prosthetic devices by a human with tetraplegia. *Nature*, 442(7099):164–71.

[Hodgkin and Huxley, 1952] Hodgkin, A. L. and Huxley, A. F. (1952). A quantitative description of membrane current and its application to conduction and excitation in nerve. *The Journal of Physiology*, 117(4):500–544.

[Horsley and Clarke, 1908] Horsley, V. and Clarke, R. H. (1908). The structure and functions of the cerebellum examined by a new method. *Brain*, 31(1):45–124.

[Hubel, 1957] Hubel, D. H. (1957). Tungsten Microelectrode for Recording from Single Units. *Science*, 125(3247):549–50.

[Hubel, 1959] Hubel, D. H. (1959). Single unit activity in striate cortex of unrestrained cats. *Journal of Physiology*, 147(2):226–238.

[Irwin et al., 2016] Irwin, Z. T., Thompson, D. E., Schroeder, K. E., Tat, D. M., Hassani, A., Bullard, A. J., Woo, S. L., Urbanchek, M. G., Sachs, A. J., Cederna, P. S., Stacey, W. C., Patil, P. G., and Chestek, C. A. (2016). Enabling Low-Power, Multi-Modal Neural Interfaces Through a Common, Low-Bandwidth Feature Space. *IEEE Transactions on Neural Systems and Rehabilitation Engineering*, 24(5):521–531.

[Jarosiewicz et al., 2015] Jarosiewicz, B., Sarma, A. A., Bacher, D., Masse, N. Y., Simeral, J. D., Sorice, B., Oakley, E. M., Blabe, C., Pandarinath, C., Gilja, V., Cash, S. S., Eskandar, E. N., Friehs, G., Henderson, J. M., Shenoy, K. V., Donoghue, J. P., and Hochberg, L. R. (2015). Virtual typing by people with tetraplegia using a self-calibrating intracortical brain-computer interface. *Science Translational Medicine*, 7(313):313ra179–313ra179.

[Johansson and Flanagan, 2009] Johansson, R. S. and Flanagan, J. R. (2009). Coding and use of tactile signals from the fingertips in object manipulation tasks. *Nature reviews. Neuroscience*, 10(5):345–59.

[Johansson et al., 1992] Johansson, R. S., Häger, C., and Bäckström, L. (1992). Somatosensory control of precision grip during unpredictable pulling loads. *Experimental Brain Research*, 89(1):204–213.

[Kane et al., 2013] Kane, S. R., Cogan, S. F., Ehrlich, J., Plante, T. D., Mccreery, D. B., and Troyk, P. R. (2013). Electrical Performance of Penetrating Microelectrodes Chronically Implanted in Cat Cortex. *IEEE Transactions on Biomedical Engineering*, 60(8):2153–2160.

[Klaes et al., 2014] Klaes, C., Shi, Y., Kellis, S., Minxha, J., Revechkis, B., and Andersen, R. A. (2014). A cognitive neuroprosthetic that uses cortical stimulation for somatosensory feedback. *Journal of Neural Engineering*, 11(5):056024–056024.

[Kohfeld, 1971] Kohfeld, D. L. (1971). Simple reaction time as a function of stimulus intensity in decibels of light and sound. *Journal of experimental psychology*, 88(2):251.

[Lebedev and Nicolelis, 2006] Lebedev, M. A. and Nicolelis, M. A. L. (2006). Brain-machine interfaces: Past, present and future. *Trends in Neurosciences*, 29(9):536–546.

[Lempka et al., 2011] Lempka, S. F., Johnson, M. D., a Moffitt, M., Otto, K. J., Kipke, D. R., and McIntyre, C. C. (2011). Theoretical analysis of intracortical microelectrode recordings. *Journal of neural engineering*, 8(4):045006–045006.

[Leuthardt et al., 2004] Leuthardt, E. C., Schalk, G., Wolpaw, J. R., Ojemann, J. G., and Moran, D. W. (2004). A brain-computer interface using electrocorticographic signals in humans. *Journal of Neural Engineering*, 1(2):63–71.

[Limnuson et al., 2014] Limnuson, K., Lu, H., Chiel, H. J., and Mohseni, P. (2014). Real-time stimulus artifact rejection via template subtraction. *IEEE Transactions on Biomedical Circuits and Systems*, 8(3):391–400.

[London et al., 2008] London, B. M., Jordan, L. R., Jackson, C. R., and Miller, L. E. (2008). Electrical Stimulation of the Proprioceptive Cortex (Area 3a) Used to Instruct a Behaving Monkey. *IEEE Transactions on Neural Systems and Rehabilitation Engineering*, 16(1):32–36.

[Marasco et al., 2011] Marasco, P. D., Kim, K., Colgate, J. E., Peshkin, M. A., and Kuiken, T. A. (2011). Robotic touch shifts perception of embodiment to a prosthesis in targeted reinnervation amputees. *Brain*, 134(3):747–758.

[McCreery et al., 1990] McCreery, D. B., Agnew, W. F., Yuen, T. G., and Bullara, L. (1990). Charge density and charge per phase as cofactors in neural injury induced by electrical stimulation. *IEEE Transactions on Biomedical Engineering*, 37(10):996–1001.

[McGill et al., 1982] McGill, K. C., Cummins, K. L., Dorfman, L. J., Berlizot, B. B., Luetkemeyer, K., Nishimura, D. G., and Widrow, B. (1982). On the nature and elimination of stimulus artifact in nerve signals evoked and recorded using surface electrodes. *IEEE Transactions on Biomedical Engineering*, 29(2):129–137.

[McGlone and Reilly, 2010] McGlone, F. and Reilly, D. (2010). The cutaneous sensory system. *Neuroscience & Biobehavioral Reviews*, 34(2):148–159.

[McNeal, 1976] McNeal, D. R. (1976). Analysis of a model for excitation of myelinated nerve. *IEEE transactions on bio-medical engineering*, 23(4):329–37.

[Mena et al., 2017] Mena, G. E., Grosberg, L. E., Madugula, S., Hottowy, P., Litke, A., Cunningham, J., Chichilnisky, E. J., and Paninski, L. (2017). Electrical stimulus artifact cancellation and neural spike detection on large multi-electrode arrays. *PLOS Computational Biology*, 13(11):e1005842–e1005842.

[Merrill et al., 2005] Merrill, D. R., Bikson, M., and Jefferys, J. G. R. (2005). Electrical stimulation of excitable tissue : Design of efficacious and safe protocols. *Journal of Neuroscience Methods*, 141(2):171–198.

[Monzee et al., 2003] Monzee, J., Lamarre, Y., and Smith, A. M. (2003). The effects of digital anesthesia on force control using a precision grip. *Journal of Neurophysiology*, 89(2):672–683.

[Mussa-Ivaldi, 2003] Mussa-Ivaldi, F. (2003). Brain–machine interfaces: Computational demands and clinical needs meet basic neuroscience. *Trends in Neurosciences*, 26(6):329–334.

[Negi et al., 2010] Negi, S., Bhandari, R., Rieth, L., and Solzbacher, F. (2010). In vitro comparison of sputtered iridium oxide and platinum-coated neural implantable microelectrode arrays. *Biomedical Materials*, 5(1):015007–015007.

[Oby et al., 2016] Oby, E. R., Perel, S., Sadtler, P. T., Ruff, D. A., Mischel, J. L., Montez, D. F., Cohen, M. R., Batista, A. P., and Chase, S. M. (2016). Extracellular voltage threshold settings can be tuned for optimal encoding of movement and stimulus parameters. *Journal of Neural Engineering*, 13(3):036009–036009.

[O'Doherty et al., 2009] O'Doherty, J. E., Lebedev, M. A., Hanson, T. L., Fitzsimmons, N. A., and Nicolelis, M. A. L. (2009). A brain-machine interface instructed by direct intracortical microstimulation. *Frontiers in Integrative Neuroscience*, 3(13):3662–3669.

[O'Doherty et al., 2011] O'Doherty, J. E., Lebedev, M. A., Ifft, P. J., Zhuang, K. Z., Shokur, S., Bleuler, H., and Nicolelis, M. A. L. (2011). Active tactile exploration using a brain-machine-brain interface. *Nature*, 479(7372):228–231.

[O'Doherty and Sabes, 2016] O'Doherty, J. E. and Sabes, P. N. (2016). Towards artificial proprioception for brain-machine interfaces. In *2016 Neuroscience Meeting Planner*, Program No. 288.08, San Diego, CA. Society for Neuroscience.

[O'Shea and Shenoy, 2018] O'Shea, D. J. and Shenoy, K. V. (2018). ERAASR: An algorithm for removing electrical stimulation artifacts from multielectrode array recordings. *Journal of Neural Engineering*, 15(2):026020.

[Otto et al., 2005a] Otto, K. J., Rousche, P. J., and Kipke, D. R. (2005a). Cortical microstimulation in auditory cortex of rat elicits best-frequency dependent behaviors. *Journal of Neural Engineering*, 2(2):42–42.

[Otto et al., 2005b] Otto, K. J., Rousche, P. J., and Kipke, D. R. (2005b). Microstimulation in auditory cortex provides a substrate for detailed behaviors. *Hearing Research*, 210:112–117.

[Pandarinath et al., 2017] Pandarinath, C., Nuyujukian, P., Blabe, C. H., Sorice, B. L., Saab, J., Willett, F. R., Hochberg, L. R., Shenoy, K. V., and Henderson, J. M. (2017). High performance communication by people with paralysis using an intracortical brain-computer interface. *eLife*, 6:1–27.

[Penfield and Boldrey, 1937] Penfield, W. and Boldrey, E. (1937). Somatic motor and sensory representation in the cerebral cortex of man as studied by electrical stimulation. *Brain*, 60(4):389–443.

[Penfield and Rasmussen, 1950] Penfield, W. and Rasmussen, T. (1950). *The Cerebral Cortex of Man; a Clinical Study of Localization of Function.* Macmillan, Oxford, England.

[Picard and Smith, 1992] Picard, N. and Smith, A. M. (1992). Primary motor cortical responses to perturbations of prehension in the monkey. *Journal of Neurophysiology*, 68(5):1882–1894.

[Piccolino, 1998] Piccolino, M. (1998). Animal electricity and the birth of electrophysiology: The legacy of Luigi Galvani. *Brain Research Bulletin*, 46(5):381–407.

[Quian Quiroga, 2009] Quian Quiroga, R. (2009). What is the real shape of extracellular spikes? *Journal of Neuroscience Methods*, 177(1):194–198.

[Quick et al., 2014] Quick, K. M., Card, N. S., Whaite, S. M., Mischel, J., Loughlin, P., and Batista, A. P. (2014). Assessing vibrotactile feedback strategies by controlling a cursor with unstable dynamics. *2014 36th Annual International Conference of the IEEE Engineering in Medicine and Biology Society, EMBC 2014*, pages 2589–2592.

[Rajan et al., 2015] Rajan, A. T., Boback, J. L., Dammann, J. F., Tenore, F. V., Wester, B. A., Otto, K. J., Gaunt, R. A., and Bensmaia, S. J. (2015). The effects of chronic intracortical microstimulation on neural tissue and fine motor behavior. *Journal of Neural Engineering*, 12(6):066018–066018.

[Ranck, 1975] Ranck, J. B. (1975). Which elements are excited in electrical stimulation of mammalian central nervous system: A review. *Brain research*, 98.

[Ranck, 1981] Ranck, J. B. (1981). Extracellular stimulation. In *Electrical Stimulation Research Techniques*, pages 1–36. Elsevier.

[Raspopovic et al., 2014] Raspopovic, S., Capogrosso, M., Petrini, F. M., Bonizzato, M., Rigosa, J., Di Pino, G., Carpaneto, J., Controzzi, M., Boretius, T., and Fernandez, E.

(2014). Restoring natural sensory feedback in real-time bidirectional hand prostheses. *Science translational medicine*, 6(222):222ra19–222ra19.

[Ratcliff, 1993] Ratcliff, R. (1993). Methods for dealing with reaction time outliers. *Psychological bulletin*, 114(3):510.

[Rattay, 1987] Rattay, F. (1987). Ways to approximate current-distance relations for electrically stimulated fibers. *Journal of theoretical biology*, 125(3):339–49.

[Rattay, 1999] Rattay, F. (1999). The basic mechanism for the electrical stimulation of the nervous system. *Neuroscience*, 89(2):335–346.

[Renshaw et al., 1940] Renshaw, B., Forbes, a., and Morison, B. R. (1940). Activity of Isocortex and Hippocampus: Electrical Studies with Micro-Electrodes. *Journal of Neurophysiology*, 3:74–105.

[Reswick et al., 1975] Reswick, J., Mooney, V., Schwartz, A., McNeal, D., Su, N., Bekey, G., Bowman, B., Snelson, R., Irons, G., Schmid, P., and others (1975). Sensory feedback prosthesis using intraneural electrodes. *Proc. of 5th ETAN*, pages 9–25.

[Rohland, 1975] Rohland, T. A. (1975). Sensory feedback for powered limb prostheses. *Medical and biological engineering*, 13(2):300–301.

[Romo et al., 2000] Romo, R., Hernández, a., Zainos, a., Brody, C. D., and Lemus, L. (2000). Sensing without touching: Psychophysical performance based on cortical microstimulation. *Neuron*, 26(1):273–278.

[Romo et al., 1998] Romo, R., Hernández, A., Zainos, A., and Salinas, E. (1998). Somatosensory discrimination based on cortical microstimulation. *Nature*, 392(6674):387–390.

[Rothwell et al., 1982] Rothwell, J. C., Traub, M. M., Day, B. L., Obeso, J. A., Thomas, P. K., and Marsden, C. D. (1982). Manual motor performance in a deafferented man. *Brain*, 105(3):515–542.

[Saal and Bensmaia, 2014] Saal, H. P. and Bensmaia, S. J. (2014). Touch is a team effort: Interplay of submodalities in cutaneous sensibility. *Trends in Neurosciences*, 37(12):689–697.

[Salzman et al., 1990] Salzman, D. C., Britten, K. H., and Newsome, W. T. (1990). Cortical microstimulation influences perceptual judgements of motion direction. *Nature*, 346(6280):174–177.

[Schiefer et al., 2016] Schiefer, M., Tan, D., Sidek, S. M., and Tyler, D. J. (2016). Sensory feedback by peripheral nerve stimulation improves task performance in individuals with upper limb loss using a myoelectric prosthesis. *Journal of Neural Engineering*, 13(1):016001.

[Schmidt, 1980] Schmidt, E. M. (1980). Single neuron recording from motor cortex as a possible source of signals for control of external devices. *Annals of Biomedical Engineering*, 8:339–349.

[Schmidt et al., 1996] Schmidt, E. M., Bak, M. J., Hambrecht, F. T., Kufta, C. V., O'Rourke, D. K., and Vallabhanath, P. (1996). Feasibility of a visual prosthesis for the blind based on intracortical microstimulation of the visual cortex. *Brain : a journal of neurology*, 119 (Pt 2:507–522.

[Schwartz et al., 2001] Schwartz, A. B., Taylor, D. M., and Helms Tillery, S. I. (2001). Extraction algorithms for cortical control of arm prosthetics. *Current Opinion in Neurobiology*, 11:701–707.

[Serruya et al., 2002] Serruya, M. D., Hatsopoulos, N. G., Paninski, L., Fellows, M. R., and Donoghue, J. P. (2002). Instant neural control of a movement signal. *Nature*, 416(6877):141–142.

[Shannon, 1979] Shannon, G. F. (1979). A myoelectrically-controlled prosthesis with sensory feedback. *Medical and Biological Engineering and Computing*, 17(1):73–80.

[Shimada et al., 2009] Shimada, S., Fukuda, K., and Hiraki, K. (2009). Rubber Hand Illusion under Delayed Visual Feedback. *PLoS ONE*, 4(7):e6185.

[Simeral et al., 2011] Simeral, J. D., Kim, S.-P., Black, M. J., Donoghue, J. P., and Hochberg, L. R. (2011). Neural control of cursor trajectory and click by a human with tetraplegia 1000 days after implant of an intracortical microelectrode array. *Journal of neural engineering*, 8(2):025027–025027.

[Smeets and Brenner, 2017] Smeets, J. B. and Brenner, E. (2017). What is the best methods to determine reaction times. In *2017 Neuroscience Meeting Planner*, Program No. 316.14, Washington, DC.

[Stark and Abeles, 2007] Stark, E. and Abeles, M. (2007). Predicting Movement from Multiunit Activity. *Journal of Neuroscience*, 27(31):8387–8394.

[Stoney et al., 1968] Stoney, S. D., Thompson, W. D., and Asanuma, H. (1968). Excitation of pyramidal tract cells by intracortical microstimulation: Effective extent of stimulating current. *Journal of neurophysiology*, 31(5):659–669.

[Sweet and Mark, 1953] Sweet, W. H. and Mark, V. H. (1953). Unipolar anodal electrolytic lesions in the brain of man and cat. *AMA Arch NeurPsych*, 70(2):224–234.

[Tabot et al., 2013] Tabot, G. A., Dammann, J. F., Berg, J. A., Tenore, F. V., Boback, J. L., Vogelstein, R. J., and Bensmaia, S. J. (2013). Restoring the sense of touch with a prosthetic hand through a brain interface. *Proceedings of the National Academy of Sciences of the United States of America*, 110(45):18279–84.

[Tabot et al., 2015] Tabot, G. A., Kim, S. S., Winberry, J. E., and Bensmaia, S. J. (2015). Restoring tactile and proprioceptive sensation through a brain interface. *Neurobiology of Disease*, 83:191–198.

[Tan et al., 2014] Tan, D. W., Schiefer, M. A., Keith, M. W., Anderson, J. R., Tyler, J., and Tyler, D. J. (2014). A neural interface provides long-term stable natural touch perception. *Science translational medicine*, 6(257):257ra138–257ra138.

[Taylor et al., 2002] Taylor, D. M., Helms Tillery, S. I., and Schwartz, A. B. (2002). Direct Cortical Control of 3D Neuroprosthetic Devices. *Science*, 296(5574):1829–1832.

[Tehovnik, 1996] Tehovnik, E. (1996). Electrical stimulation of neural tissue to evoke behavioral responses. *Journal of neuroscience methods*, 65(1):1–17.

[Teichner, 1954] Teichner, W. H. (1954). Recent studies of simple reaction time. *Psychol Bull*, 51(2):128–149.

[Teichner and Krebs, 1972] Teichner, W. H. and Krebs, M. J. (1972). Laws of the simple visual reaction time. *Psychological review*, 79(4):344.

[Torab et al., 2011] Torab, K., Davis, T., Warren, D., House, P., Normann, R., and Greger, B. (2011). Multiple factors may influence the performance of a visual prosthesis based on intracortical microstimulation: Nonhuman primate behavioural experimentation. *Journal of Neural Engineering*, 8(3):035001–035001.

[Trautmann et al., 2017] Trautmann, E. M., Stavisky, S. D., Lahiri, S., Ames, K. C., Kaufman, M. T., Ryu, S. I., Ganguli, S., and Shenoy, K. V. (2017). Accurate estimation of neural population dynamics without spike sorting. *bioRxiv*, pages 229252–229252.

[Urban, 2017] Urban, T. (2017). Neuralink and the Brain's Magical Future.

[Velliste et al., 2008] Velliste, M., Perel, S., Spalding, M. C., Whitford, A. S., and Schwartz, A. B. (2008). Cortical control of a prosthetic arm for self-feeding. *Nature*, 453(June):1098–1101.

[Venkatraman et al., 2009] Venkatraman, S., Elkabany, K., Long, J. D., Yao, Y., and Carmena, J. M. (2009). A system for neural recording and closed-loop intracortical microstimulation in awake rodents. *IEEE Transactions on Biomedical Engineering*, 56(1):15–22.

[Vidal, 1973] Vidal, J. J. (1973). Toward direct brain-computer communication. *Annual Review of Biophysics and Bioengineering*, 2(1):157–180.

[Wagenaar and Potter, 2002] Wagenaar, D. A. and Potter, S. M. (2002). Real-time multichannel stimulus artifact suppression by local curve fitting. *Journal of neuroscience methods*, 120(2):113–20.

[Wang et al., 2013] Wang, W., Collinger, J. L., Degenhart, A. D., Tyler-Kabara, E. C., Schwartz, A. B., Moran, D. W., Weber, D. J., Wodlinger, B., Vinjamuri, R. K., Ashmore,

R. C., Kelly, J. W., and Boninger, M. L. (2013). An electrocorticographic brain interface in an individual with tetraplegia. *PloS one*, 8(2):e55344–e55344.

[Wargo, 1967] Wargo, M. J. (1967). Delayed sensory feedback in visual and auditory tracking. *Perceptual and Motor Skills*, 24(1):55–62.

[Weber et al., 2012] Weber, D. J., Friesen, R., and Miller, L. E. (2012). Interfacing the Somatosensory System to Restore Touch and Proprioception: Essential Considerations. *Journal of Motor Behavior*, 44(6):403–418.

[Whelan, 2008] Whelan, R. (2008). Effective analysis of reaction time data. *The Psychological Record*, 58(3):475–482.

[Wiener, 1951] Wiener, N. (1951). Problems of sensory prosthesis. *Bulletin of the American Mathematical Society*, 57(1):27–35.

[Wodlinger et al., 2014] Wodlinger, B., Downey, J. E., Tyler-Kabara, E. C., Schwartz, a. B., Boninger, M. L., and Collinger, J. L. (2014). Ten-dimensional anthropomorphic arm control in a human brain-machine interface: Difficulties, solutions, and limitations. *Journal of neural engineering*, 12(1):016011–016011.

[Wolpaw et al., 1991] Wolpaw, J. R., McFarland, D. J., Neat, G. W., and Forneris, C. A. (1991). An EEG-based brain-computer interface for cursor control. *Electroencephalography and Clinical Neurophysiology*, 78(3):252–259.

[Yates, 1963] Yates, A. J. (1963). Delayed auditory feedback. *Psychological bulletin*, 60(3):213.

[Young et al., 2018] Young, D., Willet, F., Memberg, W. D., Murphy, B., Walter, B., Sweet, J. A., Miller, J., Hochberg, L., Kirsch, R. F., and Ajiboye, A. B. (2018). Signal processing methods for reducing artifacts in microelectrode brain recordings caused by functional electrical stimulation. *Journal of neural engineering*, 15(2):0–21.

[Zele et al., 2007] Zele, A. J., Cao, D., and Pokorny, J. (2007). Threshold units: A correct metric for reaction time? *Vision research*, 47(5):608–611.